THESIS APPROVAL

GRADUATE SCHOOL, KASETSART UNIVERSITY

Master of Engineering (Chemical Engineering)

DEGREE

Chemical Engineering	Chemical Engineering
FIELD	**DEPARTMENT**

TITLE: Effect of Non—Uniform Temperature Distribution in a One—Zone TAP Reactor on Accuracy of Estimated Gas Diffusivities and First Order Irreversible Reaction Rate Constants

NAME: Miss Kaew-arpha Thavornprasert

THIS THESIS HAS BEEN ACCEPTED BY

THESIS ADVISOR

(Associate Professor Phungphai Phanawadee, D.Sc.)

THESIS CO-ADVISOR

(Assistant Professor Attasak Jaree, Ph.D.)

DEPARTMENT HEAD

(Associate Professor Phungphai Phanawadee, D.Sc.)

APPROVED BY THE GRADUATE SCHOOL ON _____

DEAN

(Associate Professor Gunjana Theeragool, D.Agr.)

THESIS

EFFECT OF NON−UNIFORM TEMPERATURE DISTRIBUTION IN A ONE−ZONE TAP REACTOR ON ACCURACY OF ESTIMATED GAS DIFFUSIVITIES AND FIRST ORDER IRREVERSIBLE REACTION RATE CONSTANTS

KAEW−ARPHA THAVORNPRASERT

A Thesis Submitted in Partial Fulfillment of
the Requirements for the Degree of
Master of Engineering (Chemical Engineering)
Graduate School, Kasetsart University
2010

Kaew-arpha Thavornprasert 2010: Effect of Non-Uniform Temperature Distribution in a One-Zone TAP Reactor on Accuracy of Estimated Gas Diffusivities and First Order Irreversible Reaction Rate Constants. Master of Engineering (Chemical Engineering), Major Field: Chemical Engineering, Department of Chemical Engineering. Thesis Advisor: Associate Professor Phungphai Phanawadee, D.Sc. 95 pages.

The TAP transient pulse response experiment has been increasingly used for heterogeneous catalytic reaction studies. The size and shape of the TAP response contain information on gas transport and chemical kinetics. Estimation of transport and kinetic parameters from the experimental response requires mathematical models describing the processes in the TAP reactor. The models are typically based on the assumption of uniform temperature distribution in the reactor. In this work, the effect of non-uniform temperature distribution in a one-zone reactor on the accuracy of estimated diffusivities and first order irreversible reaction rate constants are theoretically investigated via simulation for non-porous catalyst pellets. The experimental responses are obtained from simulation under non-uniform temperature distribution condition. Parameter estimation is performed using the uniform temperature distribution model. Estimation methods involve both the curve fitting (least-square) method and the moment-based method applied to different types of responses including exit flow rate curves and normalized responses. Deviations of estimated parameters from real values when using different methods are compared. Simulation results show that the deviations of estimated diffusivities are not larger than 0.62% indicating that the uniform temperature distribution assumption is valid for estimation of diffusivities. The deviations of estimated reaction rate constant can be large and depend on the estimation methods. Percentage deviations of estimated reaction rate constants obtained from the curve fitting of exit flow rates are generally smaller than those from other methods. For all estimation methods, the deviations of estimated reaction rate constants increase with increasing activation energy but decrease with increasing reactor temperature.

_____ _____ ___ / ___ / ____

Student's signature Thesis Advisor's signature

ACKNOWLEDGEMENTS

I would like to express my deep and sincere gratitude to my thesis advisor, Associate Professor Dr. Phungphai Phanawadee. His broad knowledge and logical way of thinking have been of great value for me. His understanding, encouraging and personal guiding have provided a good basis for the present thesis and life.

I am deeply grateful to my thesis co-advisor, Assistant Professor Dr. Attasak Jaree, and my thesis committees, Associate Professor Dr. Penjit Srinophakun and Dr. Chanatip Samart for their valuable comments and suggestions.

My sincere thanks are due to all of my friends and colleagues, for their suggestions, support and encouragement during study and research work.

I am especially appreciated my parents, my uncles and aunts, my brothers and sisters for their heartfelt love and continuing support and encouragement throughout my life.

The financial support from the National Nanotechnology Center under the National Science and Technology Development Agency, the National Center of Excellence for Petroleum, Petrochemicals, and Advanced Materials, and the Kasetsart University Research and Development Institute is also gratefully acknowledged.

Kaew-arpha Thavornprasert

February 2010

TABLE OF CONTENTS

Page

TABLE OF CONTENTS (Continued)

Page

LIST OF TABLES

LIST OF FIGURES

LIST OF FIGURES (Continued)

LIST OF FIGURES (Continued)

LIST OF ABBREVIATIONS

A	=	cross-sectional area of the microreactor (cm^2)
$C(t,z)$	=	gas concentration (mol/cm^3)
$C^*(\tau,\xi)$	=	dimensionless gas concentration
D_e	=	effective Knudsen diffusivity (cm^2/s)
$D_e(z)$	=	effective Knudsen gas diffusivity at each reactor axial coordinate
$D_e(\xi)$	=	effective Knudsen gas diffusivity at each dimensionless reactor axial coordinate
$D_{e,\xi=0.5}$	=	effective Knudsen gas diffusivity in the middle of the reactor
$T(\xi)$	=	absolute temperature at each reactor axial coordinate (K)
$T_{\xi=0.5}$	=	absolute reactor temperature (K)
$F(t,z)$	=	dimensional exit flow rate of gas (mol/s)
$F^*(\tau,\xi)$	=	dimensionless exit flow rate of gas
L	=	microreactor length (cm)
N_p	=	number of moles or molecules of gas in the inlet pulse
t	=	time (s)
z	=	reactor axial coordinate (cm)
a_s	=	surface concentration of active sites of catalyst ($mol\ cm^2$ of catalyst)
S_v	=	surface area of catalyst per volume of catalyst (cm^{-1})
$k(z)$	=	adsorption/reaction rate constant (cm^3 of gas/mol s)
$k'(z)$	=	apparent adsorption/reaction rate constant (s^{-1})
$\bar{d}$	=	average diameter of the interstitial voids between the pellets in the reactor (cm)
R	=	gas constant (= 8.314 J/mol K)
MW	=	molecular weight

LIST OF ABBREVIATIONS (Continued)

d_{pellet} = average pellet diameter (cm)

k_0 = frequency factor (s^{-1})

E = activation energy (kJ mol^{-1})

M_i^* = i^{th} moment of the dimensionless gas exit flow rate

M_0^* = zeroth moment of the dimensionless gas exit flow rate

M_1^* = first moment of the dimensionless gas exit flow rate

X = gas conversion

p = pressure (Pa)

r_D = ratio of dimensionless reaction rate constant defined by

$$r_D \equiv \frac{D_{e,est}}{D_{e,\xi=0.5}}$$

r_κ = ratio of dimensionless reaction rate constant defined by

$$r_\kappa \equiv \exp\left\{\frac{E}{R}\left(\frac{T(\xi)-T_{\xi=0.5}}{T(\xi)\times T_{\xi=0.5}}\right)\right\}$$

ΔD_e = quantity defined by $\Delta D_e \equiv \dfrac{D_{e,est}-D_{e,\xi=0.5}}{D_{e,\xi=0.5}}$

Greek letters

$\kappa(\xi)$ = dimensionless adsorption/reaction rate constant at each dimensionless reactor axial coordinate

$\kappa_{\xi=0.5}$ = dimensionless adsorption/reaction rate constant in the middle of the reactor

$\Delta\kappa$ = quantity defined by $\Delta\kappa \equiv \dfrac{\kappa_{est}-\kappa_{\xi=0.5}}{\kappa_{\xi=0.5}}$

$\delta(z-0^+)$ = Dirac delta function placed at $z=0^+$

LIST OF ABBREVIATIONS (Continued)

$\delta(\xi - 0^+)$	=	Dirac delta function placed at $\xi = 0^+$
ε_b	=	fractional voidage of the packed-bed
τ	=	dimensionless time
τ_{res}	=	dimensionless mean residence time
τ'	=	tortuosity factor
ξ	=	dimensionless reactor axial coordinate

Subscripts

est	=	estimated parameters
exp	=	experimental or non-uniform temperature distribution condition

EFFECT OF NON−UNIFORM TEMPERATURE DISTRIBUTION IN A ONE−ZONE TAP REACTOR ON ACCURACY OF ESTIMATED GAS DIFFUSIVITIES AND FIRST ORDER IRREVERSIBLE REACTION RATE CONSTANTS

INTRODUCTION

Application of transient response techniques is becoming more widespread in heterogeneous kinetic study. Transient experiments provide more information than steady-state experiments and are particularly useful for deriving mechanistic insights into individual reaction steps of complex multistep processes. A TAP pulse response experiment has been increasingly used for catalytic gas-solid reaction study (Pérez-Ramírez and Kondratenko, 2007; Gleaves *et al.*, 2009). The TAP experiment (Gleaves *et al.*, 1988, 1997) is performed by rapidly injecting a narrow gas pulse into an evacuated microreactor containing a packed bed of particles. The pulse contains a very small amount of gas (approx. 10^{-10} mol) in comparison to conventional transient response experiments. The gas molecule travels through the packed bed by Knudsen diffusion. An important feature of this flow regime is that the diffusivities of the individual components of a gas mixture are independent of either the gas mixture composition or the pressure. The gas exiting the reactor is monitored as a function of time with a quadrupole mass spectrometer (QMS), producing a transient response at the QMS detector. Intensity of the response is proportional to the exit flow rate of the corresponding gas. The size and the shape of the response depend on the transport and kinetic processes in the reactor.

Interpretations of TAP experimental data including transport and kinetic parameter estimation require mathematical models that describe the processes in the reactor. Assumptions typically involved in the mathematical models include Dirac delta inlet flow condition, zero concentration at the reactor outlet and uniform temperature distribution in the reactor (Gleaves *et al.,* 1988, 1997; Constales *et al.*, 2006). It has been reported that the Dirac delta inlet flow condition (Constales *et al.*,

2006; Tantake *et al.*, 2007) and the zero concentration at the reactor outlet (Zou *et al.*, 1993) are valid for typical operations. Discussion on the difference of the experimental responses simulated under the uniform and non-uniform temperature distribution conditions has been given by Delgado *et al.* (2002). However, no quantitative analysis for the inaccuracy of estimated parameters has been reported. In the TAP experiments, the gas diffusivity and reaction rate constants estimated from the TAP responses are expected to be as accurate as possible in order to evaluate the catalyst performance precisely. Parameter estimation can be accomplished by curve fitting between the experimental response and the model response from which its calculation is made by assuming uniform temperature distribution. Using the method of least squares, the sum of squared differences between the experimental and the model responses is minimized. Another alternative for the parameter estimation is the use of the analytical expressions of the mean residence time or the gas conversion of the exit flow rate. In this work, the effect of non-uniform temperature distribution in the reactor on the accuracy of the estimated diffusivity and first order irreversible reaction rate constant will be theoretically analyzed by computer simulation.

OBJECTIVE

The objective of this work is to theoretically investigate the effect of non-uniform temperature distribution in a TAP microreactor on accuracy of estimated gas diffusivities and estimated first order irreversible reaction rate constants obtained from the TAP response data.

Scope

Analyses of the effect of non-uniform temperature distribution in the reactor on the accuracy of the diffusivities and first order irreversible reaction rate constants estimated from the TAP experimental responses will focus on the case in which the reactor is uniformly packed with non-porous catalyst pellets. The experimental response curves for the diffusion-only and diffusion with first order irreversible reaction are obtained by numerical simulation using the temperature profiles provided by the Heterogeneous Kinetics and Particle Chemistry Laboratory, Washington University, Saint Louis, USA. The reported temperature profiles include different temperatures of 406, 498, 601, 705, and 810 K at the middle reactor position. Relationship between the reaction rate constant and temperature is governed by Arrhenius equation. Activation energy of the first order irreversible reaction is varied up to 125 kJ mol^{-1} in accordance with the value of activation energy obtained from typical first order reactions. The gas conversion is in the range of 0.01-0.99. Parameters are estimated from the experimental responses using the uniform temperature distribution model. Curve fitting and moment-related analytical expressions for the gas conversion and the mean residence time are applied for parameter estimations.

LITERATURE REVIEW

Temporal Analysis of Products or TAP (Gleaves *et al.*, 1988, 1997) is a powerful approach for heterogeneous catalytic reaction studies (Pérez-Ramírez and Kondratenko, 2007; Gleaves *et al.*, 2010). It has been applied to study mechanisms of various heterogeneously catalyzed reactions including oxidative dehydrogenation of propane (Schuurman *et al.*, 1999; Kondratenko and Pérez-Ramírez, 2004; Kondratenko *et al.*, 2005); methane conversion to syngas (Buyevskaya *et al.*, 1996; Fathi *et al.*, 2000); ammoxidation of toluene (Konietzni *et al.*, 1999), n-butane (Rodemerck *et al.*, 1997), and propane (Olea *et al.,* 2005); ammonia oxidation (Pérez-Ramírez *et al.*, 2004, 2005; Baerns *et al.*, 2005; Kondratenko and Pérez-Ramírez, 2005); and oxidation of volatile organic compounds (Heneghan *et al.*, 1999). In addition to kinetic and mechanistic information, the TAP experiments have been used to investigate transport processes in porous materials, such as zeolites (Nijhuis *et al.*, 1999; Colaris *et al.*, 2002; Delgado *et al.*, 2004), and oxygen diffusion in metal (Dewaele *et al.*, 1998; Wang *et al.*, 1998) and metal oxide (Breitkopf, 2005) catalysts.

Several types of microreactor configurations have been applied in the TAP experiments (see Figure 1). The simplest is a one-zone reactor which its total reactor volume is uniformly packed with catalyst particles. A more common reactor configuration is a three-zone reactor in which the catalyst bed is sandwiched between beds of inert particles. The main advantage of the three-zone reactor is that the temperature distribution in the catalyst bed is more uniform. A special type of three-zone reactor is a thin-zone reactor in which the catalyst bed is very thin compared to the whole length of the reactor and a uniform gas concentration in the catalyst bed can be assumed (Shekhtman *et al.*, 1999). As a result, the catalyst activity changes uniformly during the multi-pulse experiment. The domain of system parameters providing a uniform change of catalyst has been discussed (Phanawadee *et al.*, 2003).

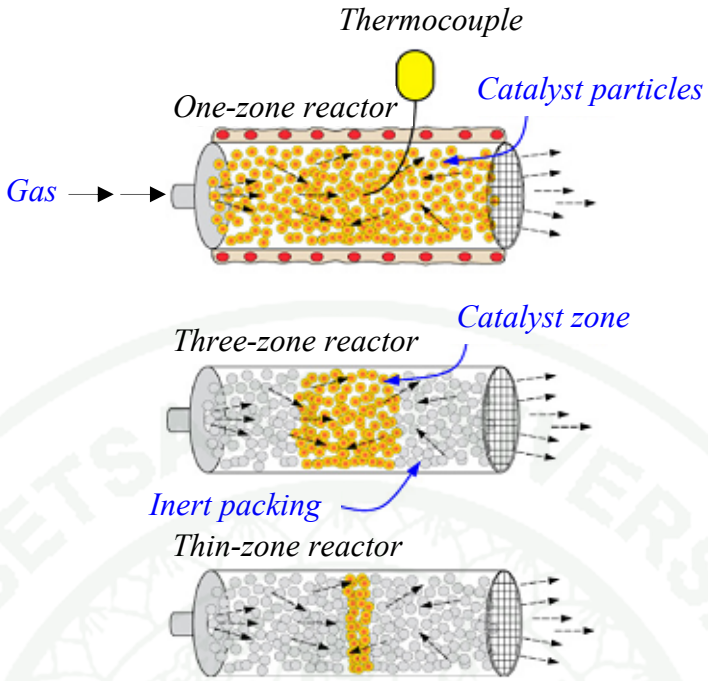

Figure 1 Examples of TAP packed-bed microreactor configuration.

Source: Gleaves *et al.* (2010)

Interpretation of TAP experimental data including transport and kinetic parameter estimation requires mathematical models describing the chemical and transport phenomena in the reactor. The mathematical models are normally based on an assumption of uniform temperature distribution in the reactor (Gleaves *et al.*, 1988, 1997; Constales *et al.*, 2006). Practically, a TAP reactor is uniformly wired with heating wire and is placed between pulse valve manifold and a vacuum chamber. Accordingly, a temperature profile in the reactor normally has a maximum. It is of great interest to investigate how the non-uniform temperature distribution affects the accuracy of estimated parameters quantitatively and to analyze the validity/invalidity of the uniform temperature distribution assumption.

When the temperature is non-uniformly distributed in the reactor, the gas diffusivity and the reaction rate constant, which are functions of temperature, are varied along the reactor axial coordinate corresponding to the temperature distribution in the reactor. In the TAP experiment, the gas transport in the reactor is dominated

by Knudsen diffusion (Gleaves *et al.*, 1988). An important characteristic of this transport process is that the diffusivities of the individual components of a gas mixture are independent of pressure, concentration, or composition of the gas mixture. The effective Knudsen diffusivity of a gas in a packed bed is proportional to the square root of temperature (T) and can be determined by (Cunningham and Williams, 1980; Huizenga and Smith, 1986)

$$D_e = \frac{\varepsilon_b}{\tau'} \frac{\bar{d}}{3} \sqrt{\frac{8RT}{\pi MW}} \tag{1}$$

where $\bar{d}$ is the average diameter of the interstitial voids between the pellets in the reactor (cm), ε_b is the void fraction in the bed, τ' is the tortuosity factor and MW is the molecular weight.

For spherical pellets,

$$\bar{d} = \frac{2\varepsilon_b}{3(1-\varepsilon_b)} d_{pellet} \tag{2}$$

where d_{pellet} is the average pellet diameter (cm).

According to Eq. (1), the effective Knudsen diffusivity of one gas can be calculated from the effective Knudsen diffusivity of another gas in the same packed bed using

$$D_{e,1} \frac{\sqrt{MW_1}}{\sqrt{T_1}} = D_{e,2} \frac{\sqrt{MW_2}}{\sqrt{T_2}} \tag{3}$$

where D_e, MW, and T are the effective Knudsen diffusivity, molecular weight, and temperature respectively, and subscripts 1 and 2 refer to gas 1 and gas 2 respectively.

As for the reaction rate constant, the relationship between the reaction rate constant and temperature follows the Arrhenius equation and is described by

$$k = k_0 \exp\left(-\frac{E}{RT}\right) \tag{4}$$

where k_0 is the frequency factor (s^{-1}), R is the gas constant (= 8.314 J/mol K), and E is the activation energy (kJ mol^{-1}).

In TAP experiments, parameter estimation can be performed by curve fitting between the experimental exit flow rate and the model exit flow rate calculated from an analytical solution or by numerical method based on least square fit. However, the use of the exit flow rate needs the information of the absolute calibration factor and the inlet pulse intensity. Typically experimental response curves are applied without converting into the exit flow rate curve. In this case, only the shape of the response is concerned and the unit-area normalized experimental response is compared with the unit-area normalized model response. Calculation of the model exit flow rate is typically made by assuming uniform temperature distribution. Analytical solutions for the exit flow rate of the gas from the one-zone reactor packed with non-porous catalysts for diffusion-only and diffusion with irreversible adsorption/reaction have been given (Gleaves *et al.*, 1988, 1997; Huinink, 1995).

Mathematical model for diffusion and irreversible adsorption/reaction in a one-zone reactor under uniform temperature distribution condition

Study in this thesis focuses on diffusion and diffusion with irreversible adsorption/reaction in a one-zone reactor. The mathematical model for the one-zone reactor packed with non-porous catalyst pellets for the uniform temperature distribution condition is based on the following assumptions (Gleaves *et al.*, 1988, 1997, 2010):

1. The catalyst bed is uniformly packed.
2. There is no radial concentration gradient in the bed and one-dimensional model is applied to describe the processes.

The mass balance equation for the diffusion of a non-reacting gas through the packed-bed under the uniform temperature distribution condition is described by (Gleaves *et al.*, 1988, 1997)

$$\varepsilon_b \frac{\partial C(t,z)}{\partial t} = D_e \frac{\partial^2 C(t,z)}{\partial z^2} \tag{5}$$

If the adsorption or reaction is first order in gas concentration, the mass balance equation for a reactant gas can be described by

$$\varepsilon_b \frac{\partial C(t,z)}{\partial t} = D_e \frac{\partial^2 C_A(t,z)}{\partial z^2} - a_s S_v (1-\varepsilon_b) k(z) C(t,z) \tag{6}$$

where $C(t,z)$ is the gas concentration in the bed (mol/cm^3), D_e is the effective Knudsen diffusivity in the bed (cm/s^2), t is the time (s), z is the axial coordinate (cm), a_s is the surface concentration of active sites of catalyst (mol cm^2 of catalyst), S_v is the surface area of catalyst per volume of catalyst (cm^{-1}), ε_b is the void fraction in the bed, and $k(z)$ is the adsorption/reaction rate constant (cm^3 of gas/mol s).

The apparent adsorption/reaction rate constant ($k'(z)$) having a unit of s^{-1} is defined by

$$k'(z) \equiv \frac{a_s S_v (1-\varepsilon_b)}{\varepsilon_b} k(z) \tag{7}$$

Hence, Eq. (6) can be rewritten as

$$\varepsilon_b \frac{\partial C(t,z)}{\partial t} = D_e \frac{\partial^2 C_A(t,z)}{\partial z^2} - \varepsilon_b k'(z) C(t,z) \tag{8}$$

The initial and boundary conditions are described by (Gleaves *et al.*, 1988, 1997)

$$t = 0;\ C(t,z) = \delta(z - 0^+)\frac{N_P}{\varepsilon_b A} \tag{9}$$

$$z = 0;\ \frac{\partial C(t,z)}{\partial z} = 0 \tag{10}$$

$$z = L; \qquad C(t,z) = 0 \tag{11}$$

where A is the cross-sectional area of the microreactor (cm^2), L is the length of the reactor (cm), N_P is the number of moles or molecules of gas in the inlet pulse (mol), and $\delta(z - 0^+)$ is the Dirac delta function placed at $z = 0^+$.

The initial condition given by Eq. (9) explains that N_P moles of gas is injected into the reactor at $t = 0$ and the corresponding gas concentration in the inlet pulse can be represented by the Dirac delta function placed at $z = 0^+$. The inlet boundary condition given by Eq. (10) corresponds to the absence of flux at the reactor entrance when the pulse valve is closed. The outlet boundary condition given by Eq. (11) specifies that the reactor outlet is held at vacuum conditions and therefore the gas concentration is zero. The gas exit flow rate ($F(t,z)$), which is the gas flux at the reactor outlet multiplied by the cross-sectional area of the reactor, determining under the uniform temperature distribution condition is described by

$$F(t,z) = -A\left(D_e \frac{\partial C(t,z)}{\partial z} \right)\Bigg|_{z=L} \tag{12}$$

where $F(t,z)$ is the exit flow rate of the gas (mol/s).

The set of Eqs. (5), (8), and (9)-(11) can be transformed to generalized dimensionless equations using dimensionless variables and parameters defined by

Dimensionless axial coordinate;

$$\xi = \frac{z}{L} \tag{13}$$

Dimensionless concentration;

$$C^*(\tau,\xi) = \frac{C(t,z)}{N_P/\varepsilon_b AL} \tag{14}$$

Dimensionless time;

$$\tau = \frac{tD_e}{\varepsilon_b L^2} \tag{15}$$

Dimensionless adsorption/reaction rate constant;

$$\kappa(\xi) = k'(z)\frac{\varepsilon_b L^2}{D_e} \tag{16}$$

Eqs. (5), (8), and (9)-(11) are then written in dimensionless form as follows:
Diffusion-only case;

$$\frac{\partial C^*(\tau,\xi)}{\partial \tau} = \frac{\partial^2 C^*(\tau,\xi)}{\partial \xi^2} \tag{17}$$

Diffusion with first order irreversible adsorption/reaction case;

$$\frac{\partial C^*(\tau,\xi)}{\partial \tau} = \frac{\partial^2 C^*(\tau,\xi)}{\partial \xi^2} - \kappa(\xi)C^*(\tau,\xi) \tag{18}$$

Dimensionless initial and boundary conditions;

$$\tau = 0; \qquad C^*(\tau,\xi) = \delta(\xi - 0^+) \tag{19}$$

$$\xi = 0; \qquad \frac{\partial C^*(\tau,\xi)}{\partial \xi} = 0 \tag{20}$$

$$\xi = 1; \qquad C^*(\tau,\xi) = 0 \tag{21}$$

The exit flow rate of the gas can be expressed in dimensionless form using the dimensionless variable defined by

$$F^*(\tau,\xi) = F(t,z)\frac{\varepsilon_b L^2}{N_P D_e} \tag{22}$$

where $F^*(\tau,\xi)$ is the dimensionless gas exit flow rate.

Eq. (12) is then written as (Gleaves *et al.*, 1997)

$$F^*(\tau,\xi) = -\left(\frac{\partial C^*(\tau,\xi)}{\partial \xi}\right)\Bigg|_{\xi=1} \tag{23}$$

The analytical solution for the dimensionless exit flow rate of the gas can be determined by applying the method of separation of variables and is described by

Diffusion-only case;

$$F^*(\tau,\xi) = \pi\sum_{n=0}^{\infty}\left\{(-1)^n(2n+1)\exp\left(-(n+0.5)^2\pi^2\tau\right)\right\} \tag{24}$$

Diffusion with first order irreversible adsorption/reaction case;

$$F^*(\tau,\xi) = \pi\exp(-\kappa\tau)\sum_{n=0}^{\infty}\left\{(-1)^n(2n+1)\exp\left(-(n+0.5)^2\pi^2\tau\right)\right\} \tag{25}$$

Eqs. (24) and (25) can be written in dimensional form as

$$\frac{F(t,z)}{N_P} = \frac{D_e\pi}{\varepsilon_b L^2}\sum_{n=0}^{\infty}\left\{(-1)^n(2n+1)\exp\left(-(n+0.5)^2\pi^2\frac{tD_e}{\varepsilon_b L^2}\right)\right\} \tag{26}$$

$$\frac{F(t,z)}{N_P} = \frac{D_e\pi}{\varepsilon_b L^2}\exp(-k'(z)t)\sum_{n=0}^{\infty}\left\{(-1)^n(2n+1)\exp\left(-(n+0.5)^2\pi^2\frac{tD_e}{\varepsilon_b L^2}\right)\right\} \tag{27}$$

The expressions describing the exit flow rate curves, Eqs. (24)-(27), are compared with experimental responses to estimate the parameters. Another alternative for parameter estimation is the use of moment or moment-related expressions of the exit flow rate which are determined assuming uniform temperature

distribution. Moment expressions for the exit flow rate for diffusion, diffusion with irreversible adsorption/reaction or with reversible adsorption have been given (Gleaves *et al.*, 1988, 1997; Huinink, 1995; Svoboda, 1993) for the one-zone reactor packed with non-porous catalyst particles.

The i[th] moment of the dimensionless gas exit flow rate (M^*_i) is defined by

$$M^*_i = \int_0^\infty F^* \tau^i d\tau \tag{28}$$

The zeroth moment is described by Eq. (29) and is unity for the diffusion-only case.

$$M^*_0 = \int_0^\infty F^* d\tau \tag{29}$$

When the irreversible adsorption/reaction occurs in the one-zone reactor packed with non-porous catalyst pellets the gas conversion can be determined by

$$X = 1 - M^*_0 = 1 - \frac{1}{\cosh\sqrt{\kappa}} = 1 - \frac{1}{\cosh\sqrt{k\varepsilon_b L^2 / D_e}} \tag{30}$$

The dimensionless mean residence time is defined by

$$\tau_{res} = \frac{M^*_1}{M^*_0} = \frac{\int_0^\infty F^* \tau d\tau}{\int_0^\infty F^* d\tau} \tag{31}$$

The expressions for the dimensionless mean residence time for the diffusion-only case and the diffusion with irreversible adsorption/reaction, respectively, are described as follows:

$$\tau_{res} = \frac{t_{res} D_e}{\varepsilon_b L^2} = 0.5 \tag{32}$$

$$\tau_{res} = \frac{\tanh\sqrt{\kappa}}{2\sqrt{\kappa}} = \frac{\tanh\sqrt{k\varepsilon_b L^2 / D_e}}{2\sqrt{k\varepsilon_b L^2 / D_e}} \tag{33}$$

Mathematical model for diffusion and irreversible adsorption/reaction in a one-zone reactor under non-uniform temperature distribution condition

When the temperature is non-uniformly distributed in the reactor, the equation describing the gas flux includes the gas diffusion and thermal diffusion terms written as (Mason *et al.*, 1963, 1967)

$$Flux = -\frac{D_e}{RT}\left(\frac{\partial p}{\partial z} - \frac{1}{2}\times p \times \frac{\partial \ln T}{\partial z}\right) \tag{34}$$

where p is the pressure (Pa) and T is the absolute temperature (K).

since $p = CRT$, Eq. (34) can also be written as

$$Flux = -D_e(z)\left(\frac{\partial C(t,z)}{\partial z} + \frac{1}{2}\times C(t,z) \times \frac{\partial \ln T(z)}{\partial z}\right) \tag{35}$$

The gas flux equation in Eq. (34) has been applied by Delgado *et al.* (2002) to develop the gas transport model for a TAP-like system called Multitrack system. The difference between the responses simulated under the uniform and non-uniform temperature distribution conditions has been reported. However, no quantitative analysis on the effect of non-uniform temperature distribution on the accuracy of the transport parameter estimated from the response has been given. The accuracy of the estimated parameters, especially the kinetic parameters, determining from the TAP experimental data is necessary. If the estimated rate constant is not correct, the estimated conversions, yields, and selectivities are not correct as well. Practically in the TAP experiments, the gas diffusivity is the basic parameter which has to be known before the kinetic parameter is estimated, consequently, the estimated diffusivity is also expected to be as accurate as possible. Therefore, it is of great interest to investigate how the non-uniform temperature distribution condition affects the accuracy of the parameters estimated from the TAP experimental response. In this study, calculation of the experimental response applies the gas flux equation described by Eq. (35). Description of the mathematical model used to calculate the

response for the non-uniform temperature distribution case will be presented in the next section.

CALCULATION METHODS

In typical TAP operations, a thermocouple is positioned in the middle of the reactor to measure the reactor temperature. All the parameters estimated from the TAP transient responses assuming uniform temperature distribution condition are reported at this temperature. In this study, the experimental responses were obtained by numerical simulation using the temperature distribution shown in Figure 2. The distribution is reported along a dimensionless reactor axial coordinate (ξ) which is the axial coordinate (z) divided by the reactor length (L).

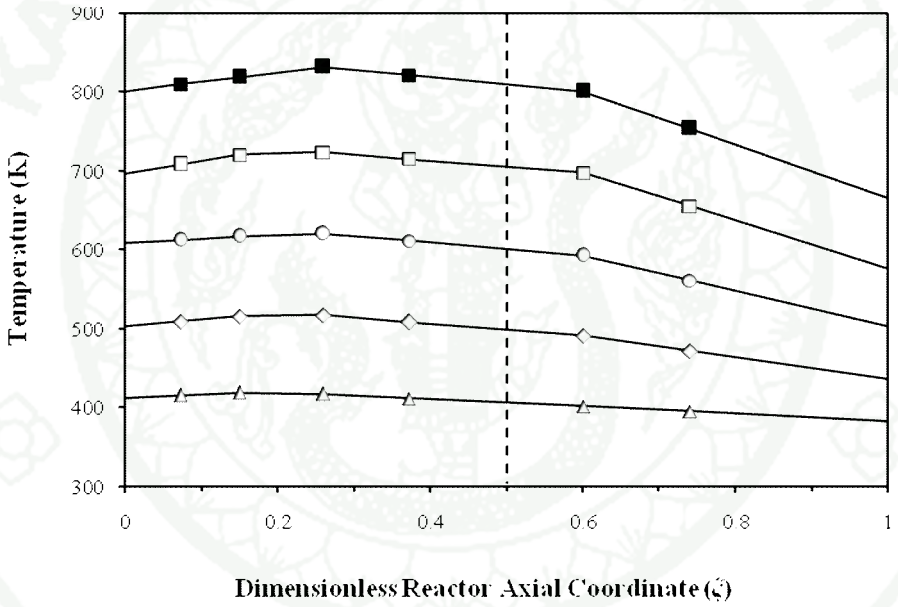

Figure 2 Temperature profiles in the TAP microreactor at the reactor temperatures equal to: 406 K (triangles), 498 K (diamonds), 601 K (circles), 705 K (squares), and 810 K (solid squares); markers on each curve represent actual measured temperature values.

These temperature profiles were provided by the Heterogeneous Kinetics and Particle Chemistry Laboratory, Washington University, Saint Louis, USA, for a TAP-1 configuration (Gleaves *et al.*, 1988). The temperatures were measured in a 4 cm long microreactor packed with 45-50 mesh silica gel particles (see the description of actual temperature values measured at different reactor positions for

a TAP-1 configuration in Appendix B). The reactor temperature was varied between 406 and 810 K. These temperature profiles are assumed to be good for both diffusion case and diffusion with first order irreversible reaction case. When reaction takes place, there may be heat of reaction involved. However, since the number of moles of reactant gas injected into the reactor is very small, the effect of heat of reaction is not significant and the temperature distribution is developed according to the reactor heating system.

To calculate the experimental response the gas diffusivity and reaction rate constant in the middle of the reactor corresponding to the reactor temperature $T(\xi = 0.5)$ are defined first. The parameters at other reactor positions are calculated from their correlation to the value at the middle position of the reactor according to Eqs. (3) and (4). In this work, the calculated distributions of the diffusivity and reaction rate constant are assumed to be real, and are used to calculate the experimental responses. The estimated parameters are determined from the simulated experimental responses assuming uniform temperature distribution condition. The estimated parameters reported as the parameters at the middle position of the reactor are then compared with the real parameters at the same reactor position. A small deviation of the estimated parameters from the real ones indicates the validity of the uniform temperature distribution assumption. Although the deviation of the estimated parameters can be determined for other axial coordinates of the reactor, the scope of this thesis is focused at the middle position of the reactor only due to the practical experimental method in which only the temperature at the middle position is reported.

Calculation of the experimental responses using the non-uniform temperature distribution model requires the gas flux equation under the non-uniform temperature distribution condition described by (Mason *et al.*, 1963, 1967)

$$Flux = -D_e(z)\left(\frac{\partial C(t,z)}{\partial z} + \frac{1}{2}\times C(t,z)\times\frac{\partial \ln T(z)}{\partial z}\right) \tag{35}$$

Assuming that the catalyst bed is uniformly packed and no radial concentration gradient is present in the catalyst zone, the mass balance equation for the gas diffusion through the packed-bed becomes

$$\varepsilon_b \frac{\partial C(t,z)}{\partial t} = \frac{\partial}{\partial z}\left(D_e(z) \frac{\partial C(t,z)}{\partial z} \right) + \frac{1}{2}\frac{\partial}{\partial z}\left(D_e(z) C(t,z) \frac{\partial \ln T(z)}{\partial z} \right) \quad (36)$$

For the diffusion with first order irreversible adsorption/reaction case, the mass balance equation can be described by

$$\varepsilon_b \frac{\partial C(t,z)}{\partial t} = \frac{\partial}{\partial z}\left(D_e(z) \frac{\partial C(t,z)}{\partial z} \right) + \frac{1}{2}\frac{\partial}{\partial z}\left(D_e(z) C(t,z) \frac{\partial \ln T(z)}{\partial z} \right) - \varepsilon_b k'(z) C(t,z) \quad (37)$$

To simplify the numerical calculation for the non-uniform temperature distribution case, we assume that the temperature is uniformly distributed within a narrow section at the reactor inlet. The initial and boundary conditions described by Eqs. (9)-(11) can then be applied. The exit flow rate of the gas ($F(t,z)$) under the non-uniform temperature distribution condition is determined by

$$F(t,z) = -A\left(D_e(z)\left(\frac{\partial C(t,z)}{\partial z} + \frac{1}{2} C(t,z) \frac{\partial \ln T(z)}{\partial z} \right) \right)\Bigg|_{z=L} \quad (38)$$

To reduce the number of computational experiments performed in this study, the model is described in a generalized dimensionless form using dimensionless variables and parameters defined by

Dimensionless axial coordinate;

$$\xi = \frac{z}{L} \quad (13)$$

Dimensionless concentration;

$$C^*(\tau,\xi) = \frac{C(t,z)}{N_P/\varepsilon_b AL} \quad (14)$$

Dimensionless time;

$$\tau = \frac{tD_{e,\xi=0.5}}{\varepsilon_b L^2} \tag{39}$$

Dimensionless adsorption/reaction rate constant;

$$\kappa(\xi) = k'(z)\frac{\varepsilon_b L^2}{D_{e,\xi=0.5}} \tag{40}$$

where $D_{e,\xi=0.5}$ is the effective Knudsen diffusivity at the middle position of the reactor (cm/s^2).

Eqs. (36) and (37) can then be written as follows:
Diffusion-only case;

$$\frac{\partial C^*(\tau,\xi)}{\partial \tau} = \frac{\partial}{\partial \xi}\left(\frac{D_e(\xi)}{D_{e,\xi=0.5}}\frac{\partial C^*(\tau,\xi)}{\partial \xi}\right) + \frac{1}{2}\frac{\partial}{\partial \xi}\left(\frac{D_e(\xi)}{D_{e,\xi=0.5}}C^*(\tau,\xi)\frac{\partial \ln T(\xi)}{\partial \xi}\right) \tag{41}$$

Diffusion with first order irreversible reaction case;

$$\frac{\partial C^*(\tau,\xi)}{\partial \tau} = \frac{\partial}{\partial \xi}\left(\frac{D_e(\xi)}{D_{e,\xi=0.5}}\frac{\partial C^*(\tau,\xi)}{\partial \xi}\right) + \frac{1}{2}\frac{\partial}{\partial \xi}\left(\frac{D_e(\xi)}{D_{e,\xi=0.5}}C^*(\tau,\xi)\frac{\partial \ln T(\xi)}{\partial \xi}\right) - \kappa(\xi)C^*(\tau,\xi) \tag{42}$$

According to Eqs. (3) and (4) the diffusivities and reaction rate constants at different positions are calculated from the defined diffusivity and reaction rate constant at the middle position of the reactor using

$$D_e(\xi) = D_{e,\xi=0.5}\frac{\sqrt{T(\xi)}}{\sqrt{T_{\xi=0.5}}} \tag{43}$$

$$\kappa(\xi) = \kappa_{\xi=0.5}\exp\left\{\frac{E}{R}\left(\frac{T(\xi)-T_{\xi=0.5}}{T(\xi)\times T_{\xi=0.5}}\right)\right\} \tag{44}$$

where $D_e(\xi)$, $\kappa(\xi)$, and $T(\xi)$ are the effective Knudsen diffusivity, dimensionless reaction rate constant, and absolute temperature at each dimensionless reactor axial coordinate respectively, and $D_{e,\xi=0.5}$, $\kappa_{\xi=0.5}$, and $T_{\xi=0.5}$ are the effective Knudsen

diffusivity, dimensionless reaction rate constant, and absolute temperature in the middle of the reactor respectively.

In this work, we define a dimensionless parameter r_κ described by

$$r_\kappa = \frac{\kappa(\xi)}{\kappa_{\xi=0.5}} \tag{45}$$

From Eq. (44), we can write

$$r_\kappa = \exp\left\{\frac{E}{R}\left(\frac{T(\xi)-T_{\xi=0.5}}{T(\xi)\times T_{\xi=0.5}}\right)\right\} \tag{46}$$

Eq. (42) can then be rewritten as

$$\frac{\partial C^*(\tau,\xi)}{\partial \tau} = \frac{\partial}{\partial \xi}\left(\frac{D_e(\xi)}{D_{e,\xi=0.5}}\frac{\partial C^*(\tau,\xi)}{\partial \xi}\right) + \frac{1}{2}\frac{\partial}{\partial \xi}\left(\frac{D_e(\xi)}{D_{e,\xi=0.5}}C^*(\tau,\xi)\frac{\partial \ln T(\xi)}{\partial \xi}\right) - r_\kappa \kappa_{\xi=0.5} C^*(\tau,\xi) \tag{47}$$

The dimensionless initial and boundary conditions are the same as those described by Eqs. (19)-(21). The gas exit flow rate can be expressed in dimensionless form using the dimensionless variable defined by

$$F^*(\tau,\xi) = F(t,z)\frac{\varepsilon_b L^2}{N_P D_{e,\xi=0.5}} \tag{48}$$

where $F^*(\tau,\xi)$ is the dimensionless gas exit flow rate.

The dimensionless exit flow rate can be calculated using

$$F^*(\tau,\xi) = -\left\{\frac{D_e(\xi)}{D_{e,\xi=0.5}}\left(\frac{\partial C^*(\tau,\xi)}{\partial \xi} + \frac{1}{2}C^*(\tau,\xi)\frac{\partial \ln T(\xi)}{\partial \xi}\right)\right\}\Bigg|_{\xi=1} \tag{49}$$

The set of Eqs. (19)-(21), (41), and (47) are numerically solved using the method of lines (MOL) (Hanna *et al.*, 1995). The partial derivatives are discretized with respect to the reactor axial coordinate, and the resulting system of ordinary

differential equations (ODEs) is solved by an initial value method. The software used in our numerical calculation is a program called LSODA (Livermore Solver for Ordinary Differential equations with Automatic method switching for stiff and non-stiff problems) (Petzold, 1983). The software is available at http://www.netlib.org. The computer programs are written in standard FORTRAN77. The programs are complied and run using the software called CYGWIN. The software is available at http://www.cygwin.com. The calculation used 1000 grids to span the axial coordinate and a time step of 0.001. The dimensionless exit flow rate curve for the non-uniform temperature distribution condition was calculated by Eq. (49) using the backward finite difference approximation.

Accuracy of the numerical calculation was investigated by comparing the dimensionless concentration ($C^*(\xi)$) profile numerically calculated under the non-uniform temperature distribution condition with that obtained from a known exact solution. This can be performed by assuming that the gas molecules do not leave the reactor and the gas flux at the reactor outlet is zero. Consequently, the outlet boundary condition becomes

$$\left(\frac{\partial C^*(\xi)}{\partial \xi}+\frac{1}{2}\times C^*(\xi)\times\frac{\partial \ln T(\xi)}{\partial \xi}\right)=0 \qquad (50)$$

We can numerically calculated $C^*(\xi)$ from the set of Eqs. (19), (20), (41), and (50). The calculated $C^*(\xi)$ as the dimensionless time (τ) approaches infinity was then compared to the exact steady-state solution of $C^*(\xi)$ given by

$$\frac{C^*(\xi_1)}{C^*(\xi_2)}=\frac{\sqrt{T(\xi_1)}}{\sqrt{T(\xi_2)}} \qquad (51)$$

Eq. (51), which has been reported by Mason *et al.* (1963), is obtained when solving Eq. (50) corresponding to the case in which the flux is zero at any axial coordinate in the reactor. The error of the numerically calculated dimensionless concentration at any reactor axial coordinate is not larger than 0.02%. In addition, the accuracy of the

numerical calculation was also investigated by checking the area of the dimensionless exit flow rate curves calculated for TAP conditions using the non-uniform temperature distribution model that must be unity according to the mass conservation. The numerical error is found to be less than 0.04%.

This study involves the analysis of the effect of non-uniform temperature distribution on accuracy of estimated diffusivities and estimated reaction rate constants. Different estimation methods are applied and the effect for those methods will be compared.

1. Effect of non-uniform temperature distribution on accuracy of estimated diffusivities

To analyze the effect of non-uniform temperature distribution on the accuracy of estimated diffusivities, the estimated diffusivity ($D_{e,est}$) reported at the middle position of the reactor is compared with the real diffusivity ($D_{e,\xi=0.5}$) at the same reactor position using ΔD_e defined by

$$\Delta D_e = \frac{D_{e,est} - D_{e,\xi=0.5}}{D_{e,\xi=0.5}} \tag{52}$$

The estimated diffusivity is determined from the experimental response obtained from simulation for an inert gas (non-reactive gas). The parameter estimation methods include the fitting of exit flow rate curves and the use of mean residence time expression of the gas exit flow rate.

1.1 Exit flow rate curve fitting

Estimation of the diffusivity using the exit flow rate curve fitting involves comparing the experimental exit flow rate curve to the model exit flow rate curve based on the least square fit. The exact solution of the model exit flow rate based on uniform temperature distribution condition is given by (Gleaves *et al.*, 1988, 1997)

$$\frac{F(t,z)}{N_P} = \frac{D_e \pi}{\varepsilon_b L^2} \sum_{n=0}^{\infty} \left\{ (-1)^n (2n+1) \exp\left(-(n+0.5)^2 \pi^2 \frac{tD_e}{\varepsilon_b L^2} \right) \right\} \tag{26}$$

The estimated parameter obtained when using the dimensional form described by Eq. (26) is $D_{e,est}$. When the dimensionless form is used in this study, the model curve is calculated using

$$F^*(\tau,\xi) = r_D \pi \sum_{n=0}^{\infty} \left\{ (-1)^n (2n+1) \exp\left(-(n+0.5)^2 \pi^2 r_D \tau \right) \right\} \tag{53}$$

where

$$r_D = \frac{D_{e,est}}{D_{e,\xi=0.5}} \tag{54}$$

In this case, the estimated parameter is r_D. The quantity ΔD_e can then be easily determined from the estimated r_D using

$$\Delta D_e = r_D - 1 \tag{55}$$

1.2 Mean residence time expression

Another alternative to determine the estimated diffusivity is to use the expression of mean residence time of the exit flow rate. The mean dimensionless residence time (τ_{res}) is determined by dividing the first moment by the zeroth moment and is described by (Gleaves et al., 1997)

$$\tau_{res} = \frac{t_{res} D_e}{\varepsilon_b L^2} = 0.5 \tag{32}$$

In our calculation the estimated diffusivity ($D_{e,est}$) is determined from the expression of the mean residence time of the experimental response ($t_{res,exp}$). Eq. (32) becomes

$$\frac{t_{res,exp} D_{e,est}}{\varepsilon_b L^2} = 0.5 \tag{56}$$

According to Eq. (39) the dimensionless mean residence time of the experimental response ($\tau_{res,exp}$) is defined by

$$\tau_{res,exp} = \frac{t_{res,exp} D_{e,\xi=0.5}}{\varepsilon_b L^2} \tag{57}$$

From Eqs. (56) and (57), we can write

$$r_D = \frac{D_{e,est}}{D_{e,\xi=0.5}} = \frac{0.5}{\tau_{res,exp}} \tag{58}$$

The quantity ΔD_e is determined from the estimated r_D using Eq. (55).

2. Effect of non-uniform temperature distribution on accuracy of estimated first order irreversible reaction rate constants

In the case of the first order irreversible adsorption/reaction, we define an indicating quantity $\Delta\kappa$, which is the deviation of the estimated reaction rate constant (κ_{est}) reported at the middle position of the reactor from the real reaction rate constant (κ_{est}) at the same reactor position corresponding to the measured reactor temperature, as

$$\Delta\kappa = \frac{\kappa_{est} - \kappa_{\xi=0.5}}{\kappa_{\xi=0.5}} \tag{59}$$

Estimation of the reaction rate constant is practically performed after the diffusivity is predetermined from the diffusion experiment. The diffusivity of the reactant gas is calculated from the diffusivity of the inert gas introduced into the reactor with the reactant gas using the correlation (Cunningham and Williams, 1980)

$$\frac{D_{e,reactant}}{D_{e,inert}} = \sqrt{\frac{MW_{inert}}{MW_{reactant}}} \tag{60}$$

where $D_{e,reactant}$ and $MW_{reactant}$ are the effective Knudsen diffusivity and molecular weight of the reactant gas respectively, $D_{e,inert}$ and MW_{inert} are the effective Knudsen diffusivity and molecular weight of the inert gas respectively. This study follows the practical procedure. Eq. (60) suggests that the estimated r_D for a reactant gas is the same as that for the inert gas previously determined. The estimated reaction rate constant was determined from the experimental response assuming uniform temperature distribution condition with the use of predetermined r_D .

Different parameter estimation methods can be applied to estimate the kinetic parameters. Those methods include the exit-flow-rate-curve fitting and the unit-area-normalized-response fitting. The two curve fitting methods are carried out by matching the experimental response to the model response based on the method of least square. The difference between these two methods is the type of response curve that is used for matching. The exit flow rate curve fitting method concerns both the size and shape of the response. The use of the exit flow rate to interpret the TAP experimental data needs the information of the absolute calibration factor and the pulse intensity required in the mathematical model (Huinink, 1995). These two parameters are not easily determined precisely and can vary depending on the operating conditions. Due to this disadvantage, another curve fitting method concerning only the shape of the response is practically more common. In this case, the unit-area normalized experimental response is compared with the unit-area normalized model response where curve fitting methods are applied to estimate the rate constant, predetermined r_D is obtained from Eq. (54) by the curve fitting method.

In addition to the least square method, the kinetic parameters can be estimated from the moment or moment-related expressions of the gas exit flow rate, i.e., the expressions of the gas conversion and the mean residence time. The gas conversion using method concerns only the size of the response while the mean residence time using method concerns only the response shape. In these cases, predetermined r_D is obtained from the moment related expression, Eq. (58).

2.1 Exit flow rate curve fitting

The exit flow rate curve fitting is performed by comparing the experimental exit flow rate curve with the model exit flow rate curve based on the least square fit. In this work, the model exit flow rate curve for the first order irreversible adsorption/reaction case is calculated using the equation

$$F^*(\tau,\xi) = r_D\pi \exp(-\kappa_{est}\tau)\sum_{n=0}^{\infty}\left\{(-1)^n (2n+1)\exp\left(-(n+0.5)^2 \pi^2 r_D \tau\right)\right\} \quad (61)$$

2.2 Unit-area normalized response fitting

The fitting of unit-area normalized responses applies the experimental response without converting into the exit flow rate curve. The model exit flow rate calculated from Eq. (61) and the experimental exit flow rate curve are unit-area normalized before matching to determine the estimated reaction rate constant.

2.3 Conversion expression

Practically in the TAP experiments, the gas conversion (X) is obtained by the use of an internal standard or an inert gas using the equation

$$X = 1 - \left\{\left(\frac{area\ of\ reactant\ gas}{area\ of\ inert\ gas}\right)_{experiment} \times \left(\frac{area\ of\ inert\ gas}{area\ of\ reactant\ gas}\right)_{inert\ bed}\right\} \quad (62)$$

The mixture of reactant and inert gases is pulsed into the reactor packed with catalyst pellets providing the experimental response. The conversion is then determined from the experimental response using the response of the same gas mixture pulsing into the bed packed with inert particles. In this work, the reaction rate constant is determined from the gas conversion expression of the simulated experimental exit flow rate curve ($F^*(\tau,\xi)$) using

$$X_{exp} = 1 - \frac{1}{\cosh\sqrt{\frac{k_{est}\varepsilon_b L^2}{D_{e,est}}}} \tag{63}$$

The conversion (X_{exp}) is calculated from the zeroth moment or the area of the experimental exit flow rate curve. According to the definition of dimensionless adsorption/reaction rate constant described by Eq. (40), Eq. (63) is written as

$$X_{exp} = 1 - \frac{1}{\cosh\sqrt{\kappa_{est} / r_D}} \tag{64}$$

2.4 Mean residence time expression

The expression for the dimensionless mean residence time for the first order irreversible adsorption/reaction case is described by (Gleaves et al., 1997)

$$\tau_{res} = \frac{\tanh\sqrt{\kappa}}{2\sqrt{\kappa}} = \frac{\tanh\sqrt{k\varepsilon_b L^2 / D_e}}{2\sqrt{k\varepsilon_b L^2 / D_e}} \tag{33}$$

In this work, the reaction rate constant is determined from the dimensionless mean residence time of the experimental response ($\tau_{res,exp}$). Eq. (33) becomes

$$\tau_{res,exp} = \frac{\tanh\sqrt{k_{est}\varepsilon_b L^2 / D_{e,est}}}{2\sqrt{k_{est}\varepsilon_b L^2 / D_{e,est}}} \tag{65}$$

According to Eq. (40), Eq. (65) can be written as

$$\tau_{res,exp} = \frac{\tanh\sqrt{\kappa_{est} / r_D}}{2\sqrt{\kappa_{est} / r_D}} \tag{66}$$

RESULTS AND DISCUSSION

This section will present the simulation results obtained from the quantitative analysis of the effect of non-uniform temperature distribution on the accuracy of estimated diffusivities and reaction rate constants. Deviations of estimated parameters from real values when using different estimation methods will be compared.

1. Effect of non-uniform temperature distribution on accuracy of estimated diffusivities

In this study, the exit-flow-rate-curve-fitting and the use of mean residence time expression of the gas exit flow rate are applied to estimate the diffusivities. Using the exit-flow-rate-curve-fitting method, the sum of squared differences between the simulated experimental and the model exit flow rate curves are minimized based on the least square fit, providing r_D in Eq. (54). A comparison between the simulated experimental and the model exit flow rate curves corresponding to the reactor temperature of 810 K is shown in Figure 3. The agreement between the two curves is excellent. The 95% confidence interval for the estimated diffusivities ($D_{e,est}$) or r_D from the curve fitting of each calculation for all reactor temperatures is narrow within ±0.008% of the estimated diffusivities. The excellent fit between the simulated and model curves are also obtained for other reactor temperatures.

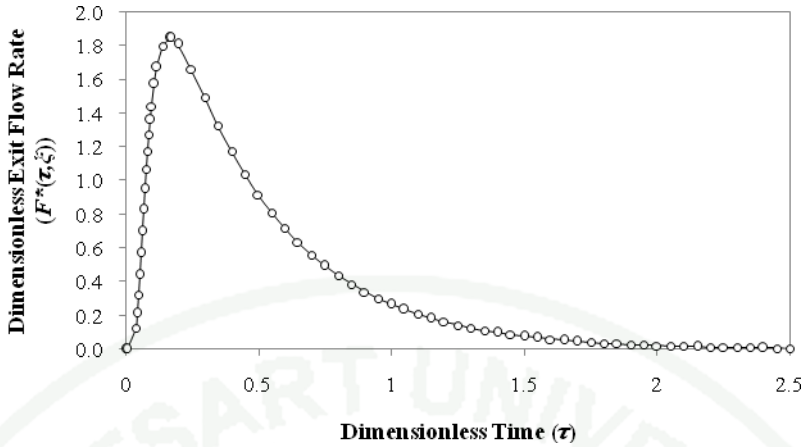

Figure 3 Comparison of the simulated experimental exit flow rate curve (circles) with the model exit flow rate curve (line) for the exit-flow-rate-curve-fitting method**.**

The estimated diffusivities are also determined from the moment expression of the experimental exit flow rate. For the diffusion-only case, the mean residence is applied as a moment-related quantity. The parameter r_D is obtained when the mean residence time of the experimental exit flow rate curve equates with the estimated diffusivity. Figure 4 shows the comparison between the simulated experimental and model exit flow rate curves when the mean residence time expression is applied to estimate the diffusivity. The comparison shown in Figure 4 corresponds to the reactor temperature of 406 K for which the error of estimated diffusivity is largest. In this case, the estimated r_D obtained from Eq. (58) is substituted into Eq. (53) to generate the model exit flow rate curve. Similarly to the curve fitting method, the excellent fit between the simulated and model curves are also obtained for the comparisons at other reactor temperatures.

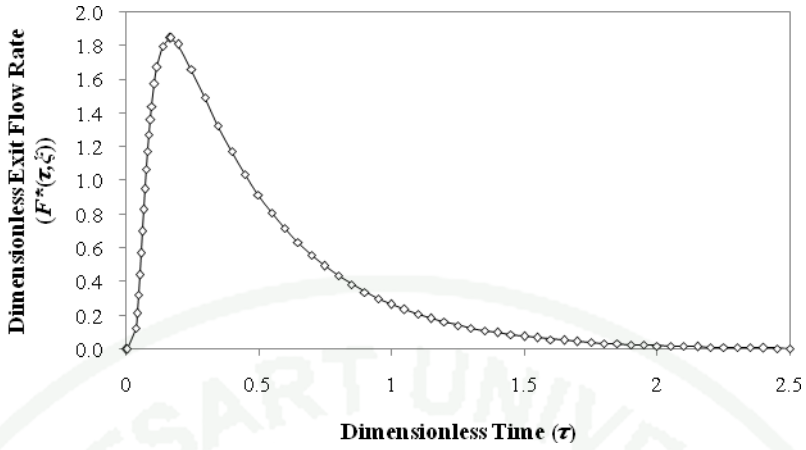

Figure 4 Comparison of the simulated experimental exit flow rate curve (diamonds) with the model exit flow rate curve (line) for the mean-residence-time-expression-using method.

Calculated values of r_D and ΔD_e obtained from the exit-flow-rate-curve-fitting and the mean-residence-time-expression-using methods for different reactor temperatures are presented in Table 1. Both estimation methods overestimate the diffusivity at the reactor temperatures of 406 and 498 K but underestimate the diffusivity at the reactor temperatures of 705 and 810 K. The magnitudes of $|\Delta D_e|$ obtained from the exit-flow-rate-curve-fitting method are smaller than those obtained from the mean-residence-time-expression-using method for the reactor temperatures of 406, 498, and 601 K but are larger for the reactor temperatures of 705 and 810 K. The quantities ΔD_e obtained from both methods are not larger than 0.62%.

Table 1 Calculated values of r_D and ΔD_e obtained from the exit-flow-rate-curve-fitting and the mean-residence-time-expression-using methods for different reactor temperatures.

$T_{\xi=0.5}$ (K)	r_D [b]		ΔD_e	
	Exit-flow-rate-curve-fitting	Mean-residence-time-expression-using	Exit-flow-rate-curve-fitting	Mean-residence-time-expression-using
406	1.004534±0.000038[a]	1.006194	0.004534	0.006194
498	1.001568±0.000066	1.004856	0.001568	0.004856
601	0.999134±0.000077	1.002922	-0.000866	0.002922
705	0.995664±0.000078	0.999436	-0.004336	-0.000564
810	0.994988±0.000074	0.998608	-0.005012	-0.001392

[a] 95% confidence interval, [b] ratio of the gas diffusivity defined by $r_D \equiv \frac{D_{e,est}}{D_{e,\xi=0.5}}$

In the Knudsen diffusion regime, the diffusivity is proportional to the square-root of temperature (Cunningham and Williams, 1980). The ratio of the highest temperature (T_h) to the lowest temperature (T_l) for each reactor temperature profile was investigated. Table 2 shows the quantity $\left(T_h/T_l\right)^{\frac{1}{2}}$ which is equal to the ratio of the diffusivity at the highest temperature position ($D_{e,h}$) to the diffusivity at the lowest temperature position ($D_{e,l}$). Calculation results for $D_{e,h}/D_{e,l}$ show that the differences of diffusivities at the highest and the lowest temperature positions do not exceed 12%. The shape of the temperature profile with small difference in diffusivity along the reactor axial coordinate therefore provides small magnitude of $\left|\Delta D_e\right|$. The small magnitudes of $\left|\Delta D_e\right|$ indicate that the uniform temperature distribution assumption is valid for estimation of diffusivities.

Table 2 Highest and lowest temperatures and corresponding ratios of $(T_h/T_l)^{\frac{1}{2}}$ or $D_{e,h}/D_{e,l}$ for different reactor temperatures.

$T_{\xi=0.5}$ (K)	T_h (K)	T_l (K)	$(T_h/T_l)^{\frac{1}{2}}$ or $D_{e,h}/D_{e,l}$
406	419	383	1.04
498	517	436	1.09
601	620	502	1.11
705	723	576	1.12
810	831	665	1.12

2. Effect of non-uniform temperature distribution on accuracy of estimated first order irreversible reaction rate constants

To determine the reaction rate constants, different estimation methods including the exit-flow-rate-curve fitting, the unit-area-normalized-response fitting, and the use of conversion and mean residence time expressions of the gas exit flow rate are applied. When using the exit-flow-rate-curve-fitting method, the simulated experimental and model exit flow rate curves are compared based on the method of least square fit providing the estimated reaction rate constants (κ_{est}). The comparison between the experimental and model exit flow rate curves for the reactor temperature of 406 K when $\kappa_{\xi=0.5}$ equals to 2 and E equals to 125 kJ mol^{-1} for the exit-flow-rate-curve-fitting method is shown in Figure 5. The 95% confidence interval for the estimated rate constant from the curve fitting is narrow within ±0.24% of the estimated rate constant. It can be seen from the figure that the experimental exit flow rate curve fits well with the model curve despite the very large error of estimated reaction rate constant.

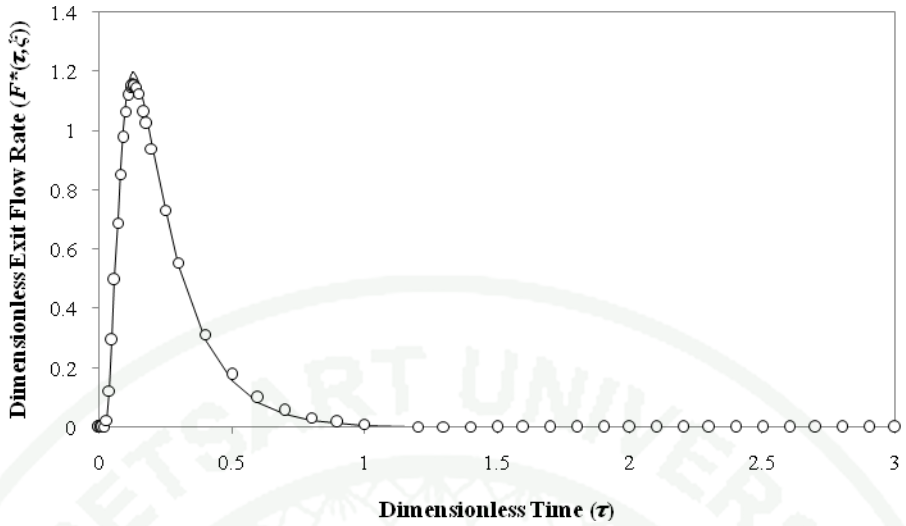

Figure 5 Comparison of the simulated experimental exit flow rate curve (line) with the model exit flow rate curve (circles) for the exit-flow-rate-curve-fitting method for $T_{\xi=0.5}$ = 406 K at $\kappa_{\xi=0.5}$ = 2 ($\Delta\kappa$ = 64.18 %), E = 125 kJ mol^{-1}.

Another curve fitting method applied to estimate the reaction rate constants involves comparing the unit-area normalized experimental exit flow rate curve with the unit-area normalized model exit flow rate curve based on the least square fit. The comparison between the unit-area normalized experimental response (dashed line) and the unit-area normalized model response (open triangles) when using the unit-area-normalized-response-fitting method for $T_{\xi=0.5}$ = 406 K at $\kappa_{\xi=0.5}$ = 2 and E = 125 kJ mol^{-1} is shown in Figure 6. The good agreement between the two unit-area normalized responses is observed. The 95% confidence interval for the estimated rate constant from the curve fitting is narrow within ±0.17% of the estimated rate constant. Figure 6 also shows the comparison between the simulated experimental exit flow rate curve (line) and model exit flow rate curve (open circles) for $T_{\xi=0.5}$ = 406 K at $\kappa_{\xi=0.5}$ = 2 and E = 125 kJ mol^{-1}. The model curve is recalculated from Eq. (61) using the predetermined r_D obtained from Eq. (54) by the curve fitting method and the estimated κ_{est} determined from the fitting of unit-area normalized responses.

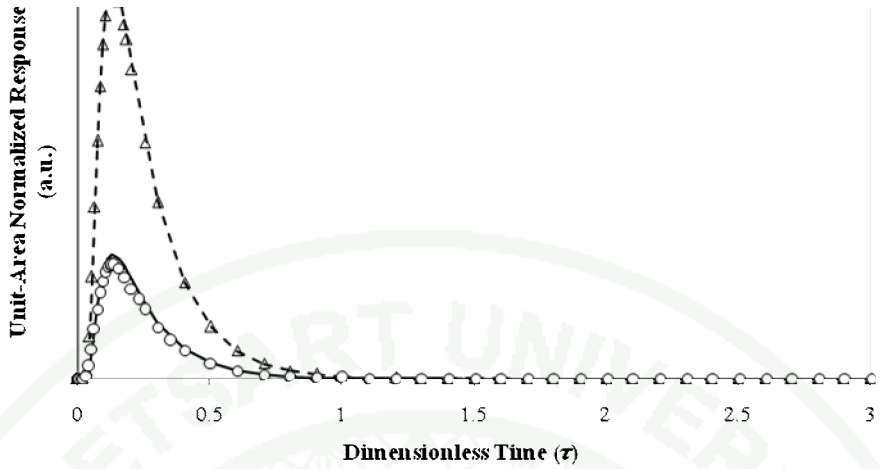

Figure 6 Comparison of the unit-area normalized experimental response (dashed line) with the unit-area normalized model response (open triangles) and comparison of the simulated experimental exit flow rate curve (line) with the model exit flow rate curve (open circles) for the unit-area-normalized-response-fitting method for $T_{\xi=0.5}$ = 406 K at $\kappa_{\xi=0.5}$ = 2 ($\Delta\kappa$ = 81.91 %), E = 125 kJ mol^{-1}.

For the conversion-expression-using method, the estimated reaction rate constant is determined from the conversion expression using Eq. (64). The parameter κ_{est} is obtained when the conversion of the experimental exit flow rate curve equates with the estimated reaction rate constant based on the method of moments. The estimated parameter is substituted into Eq. (61) to generate the model exit flow rate curve applying the predetermined r_D obtained from the moment related expression, Eq. (58). The model curve is then compared with the experimental curve to investigate whether the conversion-expression-using method can be used to estimate the reaction rate constants. The comparison between the simulated experimental and model exit flow rate curves for the conversion-expression-using method for the reactor temperature of 406 K when $\kappa_{\xi=0.5}$ equals to 2 and E equals to 125 kJ mol^{-1} is shown in Figure 7. The agreement between the two curves is good.

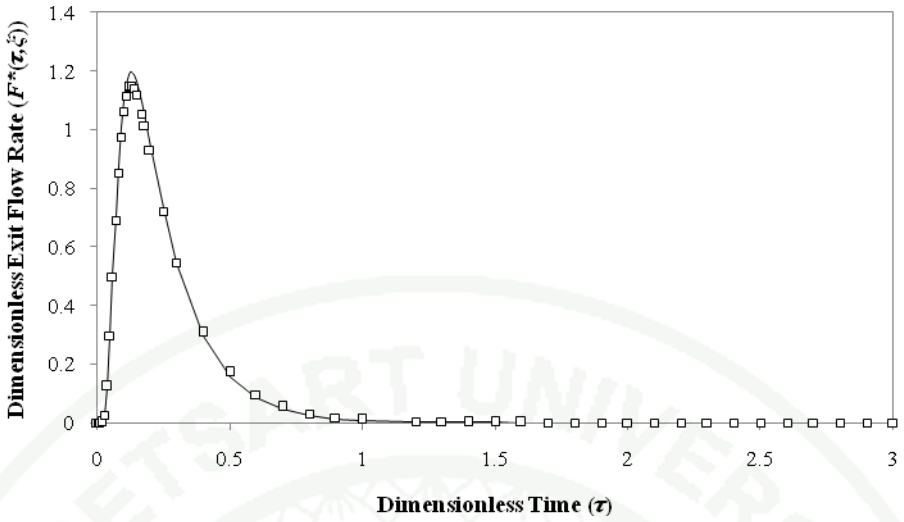

Figure 7 Comparison of the simulated experimental exit flow rate curve (line) with the model exit flow rate curve (squares) for the conversion-expression-using method for $T_{\xi=0.5}$ = 406 K at $\kappa_{\xi=0.5}$ = 2 ($\Delta\kappa$ = 67.18 %), E = 125 kJ mol^{-1}.

Another moment-based method involves the use of mean residence time expression of the experimental response described by Eq. (66) to determine the reaction rate constant. The comparison between the simulated experimental and model exit flow rate curves for the reactor temperature of 406 K when $\kappa_{\xi=0.5}$ equals to 2 and E equals to 125 kJ mol^{-1} is shown in Figure 8. The good agreement between the two curves is also observed for the mean-residence-time-using method.

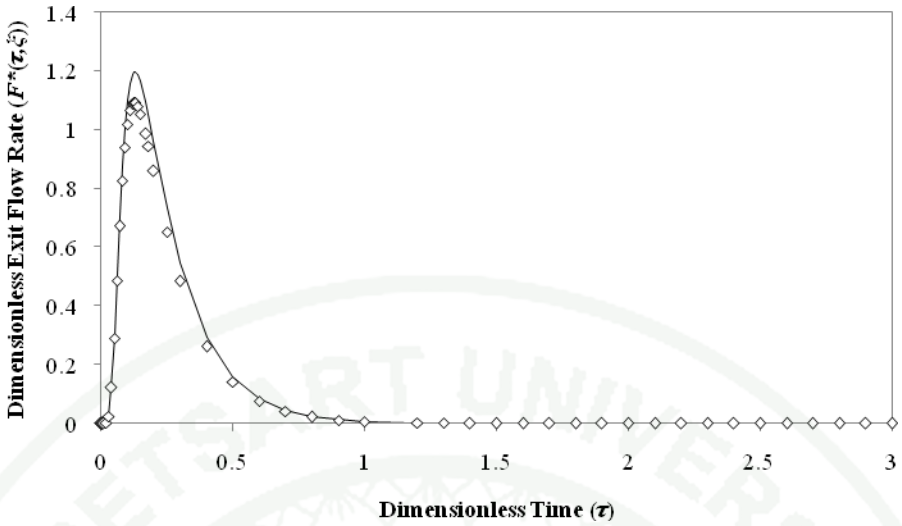

Figure 8 Comparison of the simulated experimental exit flow rate curve (line) with the model exit flow rate curve (diamonds) for the mean-residence-time-expression-using method for $T_{\xi=0.5}$ = 406 K at $\kappa_{\xi=0.5}$ = 2 ($\Delta\kappa$ = 87.01 %), E = 125 kJ mol^{-1}.

The plots shown in Figures 5-8 corresponds to the reactor temperature of 406 K when the activation energy equals to 125 kJ mol^{-1} at which the percentage differences between the estimated and real rate constants ($\Delta\kappa$ (%)) obtained from all estimation methods are very large. For the cases in which the magnitudes of $|\Delta\kappa(\%)|$ for all methods are very small, the excellent agreement between the simulated and model exit flow rate curves are obtained as shown in Figures 9(a)-9(d). The comparisons between the simulated experiment and model exit flow rate curves for different estimation methods at other reactor temperatures, conversions, and activation energy values also show the good agreement.

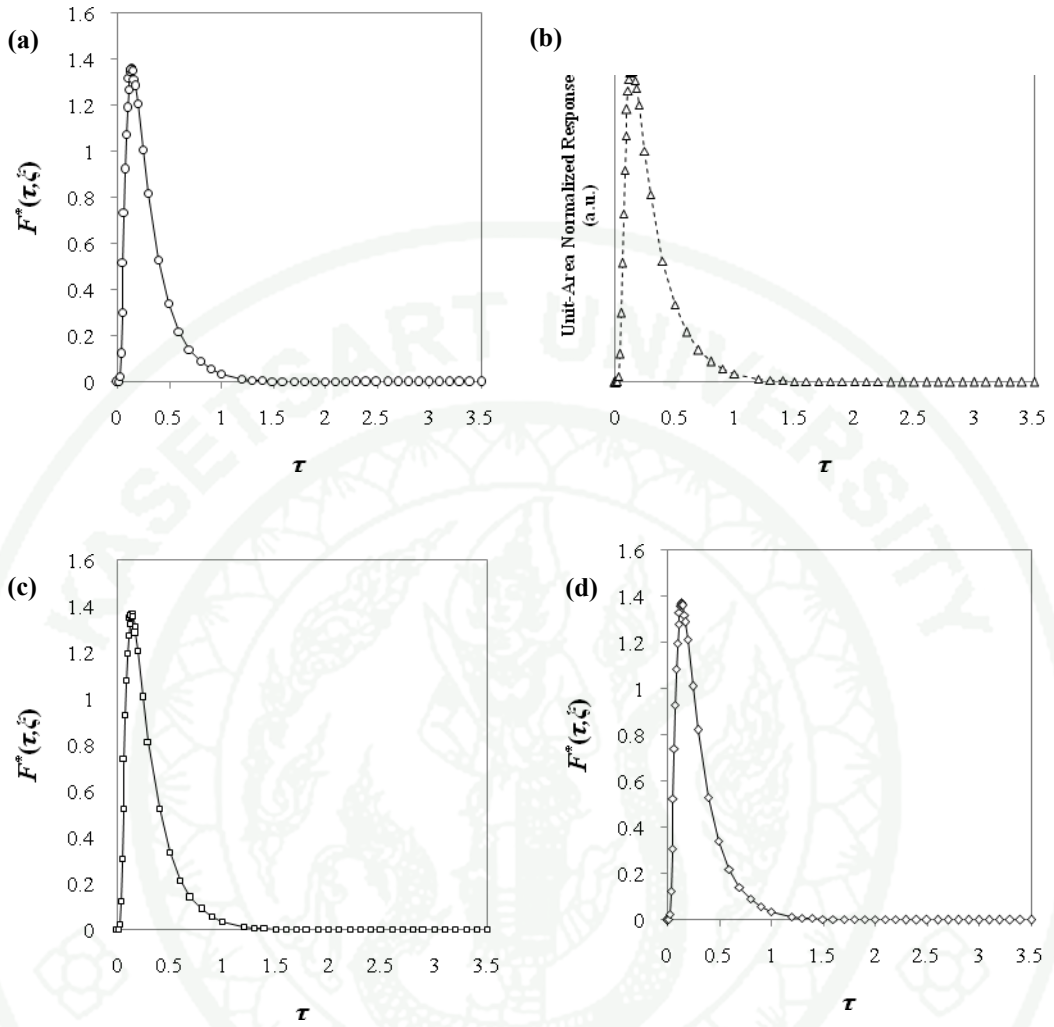

Figure 9 Comparison of the simulated experimental exit flow rate curve with the model exit flow rate curves obtained from different estimation methods: (a) exit-flow-rate-curve-fitting ($\Delta\kappa$ (%) = -0.74), unit-area-normalized-response-fitting ($\Delta\kappa$ (%) = -0.53), conversion-expression-using ($\Delta\kappa$ (%) = 0.03), and mean-residence-time-expression-using ($\Delta\kappa$ (%) = -1.22) for $T_{\xi=0.5}$ = 810 K at $\kappa_{\xi=0.5}$ = 2, E = 1 kJ mol^{-1}.

Although the agreement between the simulated experimental exit flow rate curve and the model exit flow rate curves are obtained, each estimation method does not provide the same accuracy of the estimated reaction rate constants. Percentage deviation of the estimated reaction rate constants from real values when using different estimation methods are presented in Figures 10-13. The effect of non-uniform temperature distribution on the accuracy of estimated reaction rate constants is compared for those methods.

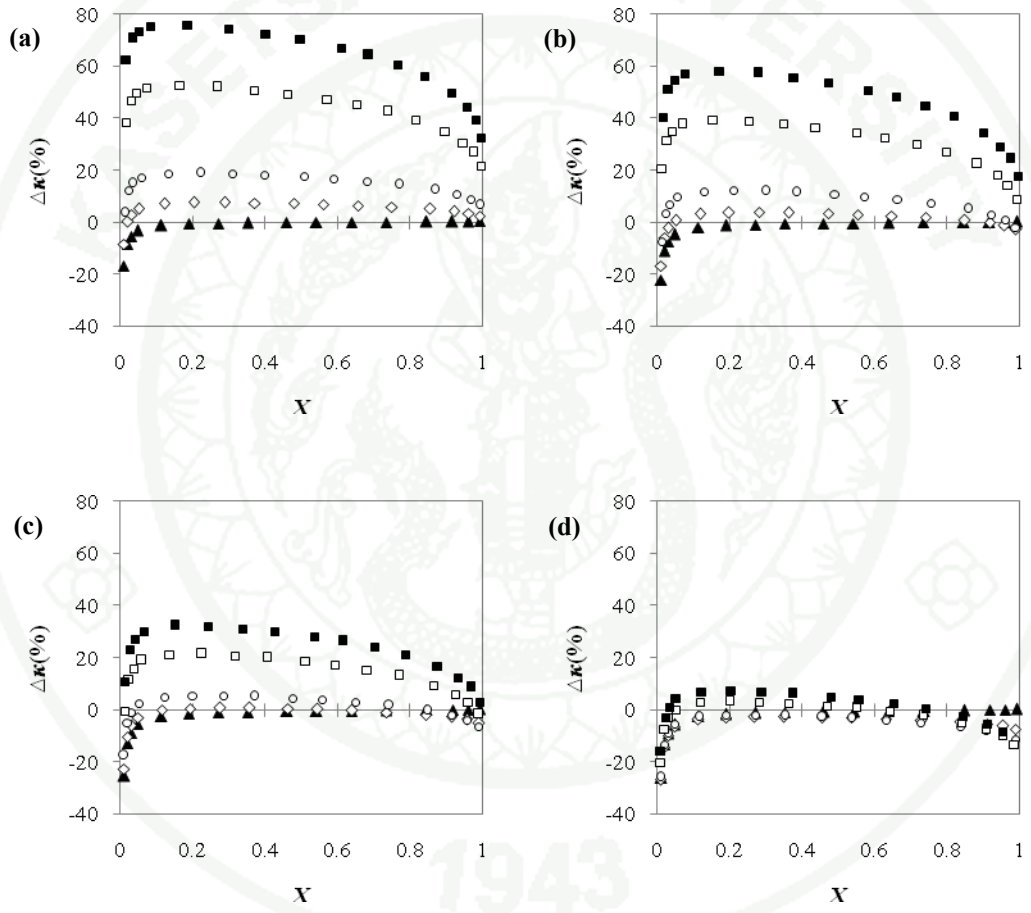

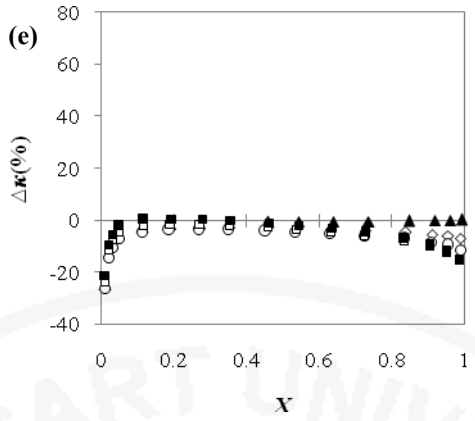

Figure 10 Plots of $\Delta\kappa$ (%) vs. conversion (X) for $T_{\xi=0.5}$ of 406 K (a), 498 K (b), 601 K (c), 705 K (d), and 810 K (e) at E = 1 kJ mol^{-1} (solid triangles), 25 kJ mol^{-1} (open diamonds), 50 kJ mol^{-1} (open circles), 100 kJ mol^{-1} (open squares), and 125 kJ mol^{-1} (solid squares) for the exit-flow-rate-curve-fitting method.

At fixed activation energy, $\Delta\kappa$ (%) depends on $\kappa(\xi)$. However, it would be better to show $\Delta\kappa$ (%) dependence on conversion (X) which is the primary characteristics of the reactive response. Figure 10 shows the plots of $\Delta\kappa$ (%) vs. conversion (X) for the reactor temperatures of 406, 498, 601, 705, and 810 K when the activation energy equals to 1, 25, 50, 100, and 125 kJ mol^{-1} for the exit-flow-rate-curve-fitting method. It is noted that, for the plot of each value of activation energy, markers shown in the plot represent different conversions corresponding to different values of κ_{real} or $\kappa_{\xi=0.5}$ defined to calculate the experimental response.

The deviations of estimated reaction rate constants ($\Delta\kappa(\%)$) obtained when using the exit-flow-rate-curve-fitting method for $T_{\xi=0.5}$ of 406 K at the conversions between 1 and 99% at different values of activation energy are presented in Figure 10(a). At E = 1 kJ mol^{-1} (solid triangles), the quantities $\Delta\kappa(\%)$ change significantly with conversion at the conversion range between 1 and 5%. $|\Delta\kappa(\%)|$ at 5% conversion is approximately 3.4% which is much smaller than that at 1% conversion ($|\Delta\kappa(\%)|$ = 17%). The large $|\Delta\kappa(\%)|$ at low conversions is due to the

small κ_{real} or $\kappa_{\xi=0.5}$. The magnitudes of $|\Delta\kappa(\%)|$ obtained at the conversions between 5 and 99% are small within which $|\Delta\kappa(\%)|$ does not exceed 1.4%.

When the activation energy is increased, the magnitudes of $|\Delta\kappa(\%)|$ increase with increasing activation energy due to the strong dependence of the reaction rate constant on activation energy in accordance with Arrhenius equation as expected. At E = 25 (open diamonds), 50 (open circles), 100 (open squares), and 125 (solid squares) kJ mol^{-1}, the significant change of $|\Delta\kappa(\%)|$ is also observed in the low conversions range. At the conversion range between 5 and 99%, the quantities $\Delta\kappa$ (%) decrease with increasing conversion. It is found that at high activation energy values (E = 100 and 125 kJ mol^{-1}), the change of $|\Delta\kappa(\%)|$ with conversion is also significant in the high conversions range.

Figures 10(b) and 10 (c) show the plots of $\Delta\kappa$ (%) at the conversions between 1 and 99% at different values of activation energy for $T_{\xi=0.5}$ of 498 and 601 K respectively. Similarly to Figure 10(a), the quantities $\Delta\kappa(\%)$ change significantly with conversion at the range of conversion between 1 and 5% for all activation energy values. At E = 1, 25, and 50 kJ mol^{-1}, $|\Delta\kappa(\%)|$ at other conversions are considerably small. $\Delta\kappa(\%)$ decreases with increasing conversion at E = 100 and 125 kJ mol^{-1} and is also change significantly with conversion when the conversion is very high. Figure 10(d) for $T_{\xi=0.5}$ of 705 K and Figure 10(e) for $T_{\xi=0.5}$ of 810 K show that the quantities $\Delta\kappa$ (%) also change significantly with conversion when the conversion is very low. However, the magnitudes of $|\Delta\kappa(\%)|$ at the conversion range between 5 and 99% are considerably small for all activation energy values for $T_{\xi=0.5}$ = 705 and 810 K.

According to Figure 10, it can be seen that the quantities $\Delta\kappa(\%)$ obtained from the exit-flow-rate-curve-fitting method can be either positive or negative values. The value of $\Delta\kappa(\%) < 0$ corresponds to an underestimation of the reaction rate constant and the value of $\Delta\kappa(\%) > 0$ corresponds to an overestimation.

Consequently, the exit-flow-rate-curve-fitting method generally overestimates the reaction rate constants for $T_{\xi=0.5}$ of 406, 498, and 601 K but underestimates the reaction rate constants for $T_{\xi=0.5}$ of 705 and 810 K.

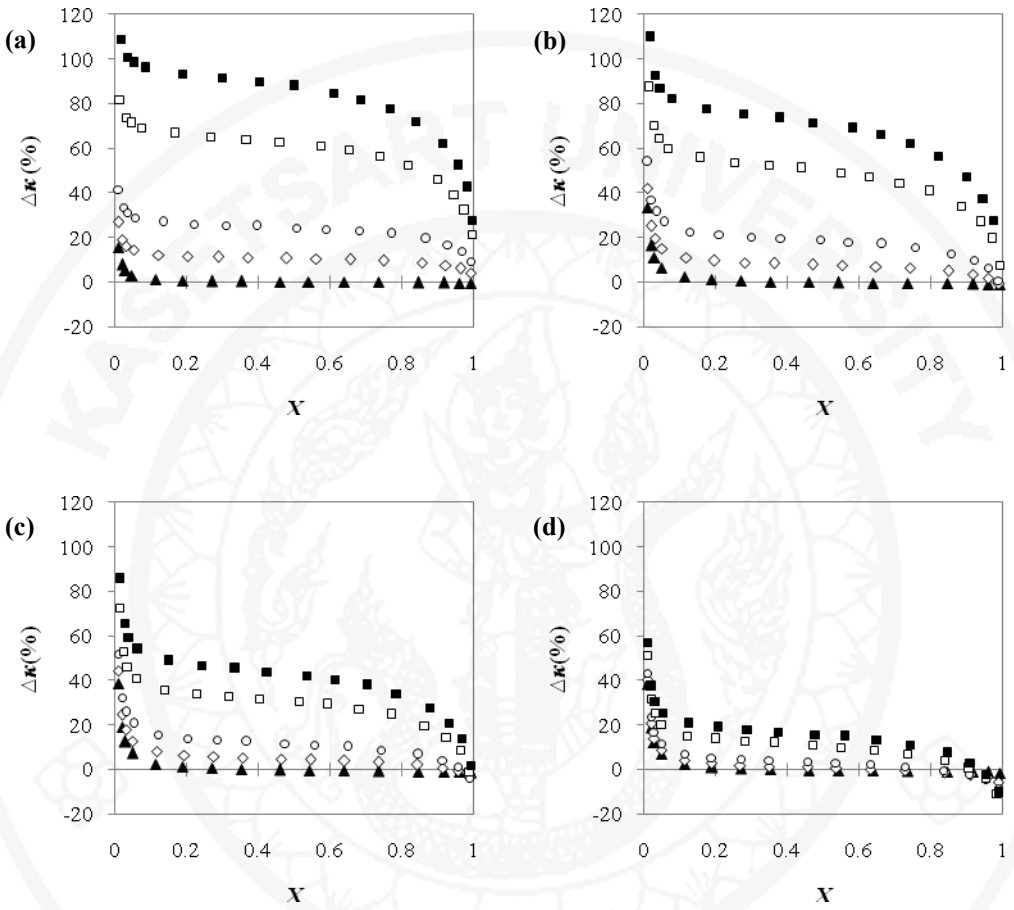

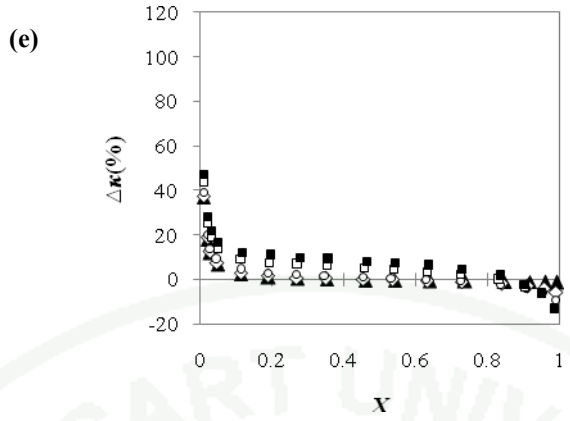

Figure 11 Plots of $\Delta\kappa$ (%) vs. conversion (X) for $T_{\xi=0.5}$ of 406 K (a), 498 K (b), 601 K (c), 705 K (d), and 810 K (e) at E = 1 kJ mol^{-1} (solid triangles), 25 kJ mol^{-1} (diamonds), 50 kJ mol^{-1} (circles), 100 kJ mol^{-1} (squares), and 125 kJ mol^{-1} (solid squares) for the unit-area-normalized-response-fitting method.

Figure 11 shows the plots of $\Delta\kappa$ (%) vs. conversion (X) for $T_{\xi=0.5}$ of 406, 498, 601, 705, and 810 K when E equals to 1, 25, 50, 100, and 125 kJ mol^{-1} for the unit-area-normalized-response-fitting method. The information of $\Delta\kappa$ (%) at the conversions between 1 and 99% at different values of E for $T_{\xi=0.5}$ of 406 K is shown in Figure 11(a). At E = 1 kJ mol^{-1} (solid triangles), the quantities $\Delta\kappa$(%) change drastically with conversion at the conversion range between 1 and 11%. $|\Delta\kappa(\%)|$ at 11% conversion is approximately 1.3% which is much smaller than that at 1% conversion ($|\Delta\kappa(\%)|$ = 15.6%). The magnitudes of $|\Delta\kappa(\%)|$ obtained at other conversions are small within which $|\Delta\kappa(\%)|$ does not exceed 1%. When the activation energy is increased, the magnitudes of $|\Delta\kappa(\%)|$ increase with increasing activation energy as expected. At E = 25 (open diamonds), 50 (open circles), 100 (open squares), and 125 (solid squares) kJ mol^{-1}, the significant change of $|\Delta\kappa(\%)|$ is also observed in the low conversions range. At the conversion range between 11 and 99%, the quantities $\Delta\kappa$ (%) decrease with increasing conversion.

It is found that at E = 50, 100, and 125 kJ mol^{-1}, $|\Delta\kappa(\%)|$ also changes significantly with conversion in the very high conversions range. Similar plots of $\Delta\kappa$ (%) vs. conversion at different values of activation energy are obtained for $T_{\xi=0.5}$ of 498, 601, 705, and 810 K as shown in Figures 11(b), 11(c), 11(d), and 11(e) respectively. In addition, the unit-area-normalized-response-fitting method generally overestimates the reaction rate constants for all reactor temperatures.

Both the exit-flow-rate-curve-fitting and the unit-area-normalized-response-fitting methods are based on the least square fit between the simulated and model curves. It is found that the magnitudes of $|\Delta\kappa(\%)|$ obtained from the fitting of unit-area-normalized responses are generally higher than those from the exit-flow-rate-curve-fitting method, since the unit-area-normalized-response-fitting method does not take into account the size of the response while the exit flow rate curve fitting concerns both the size and the shape of the response.

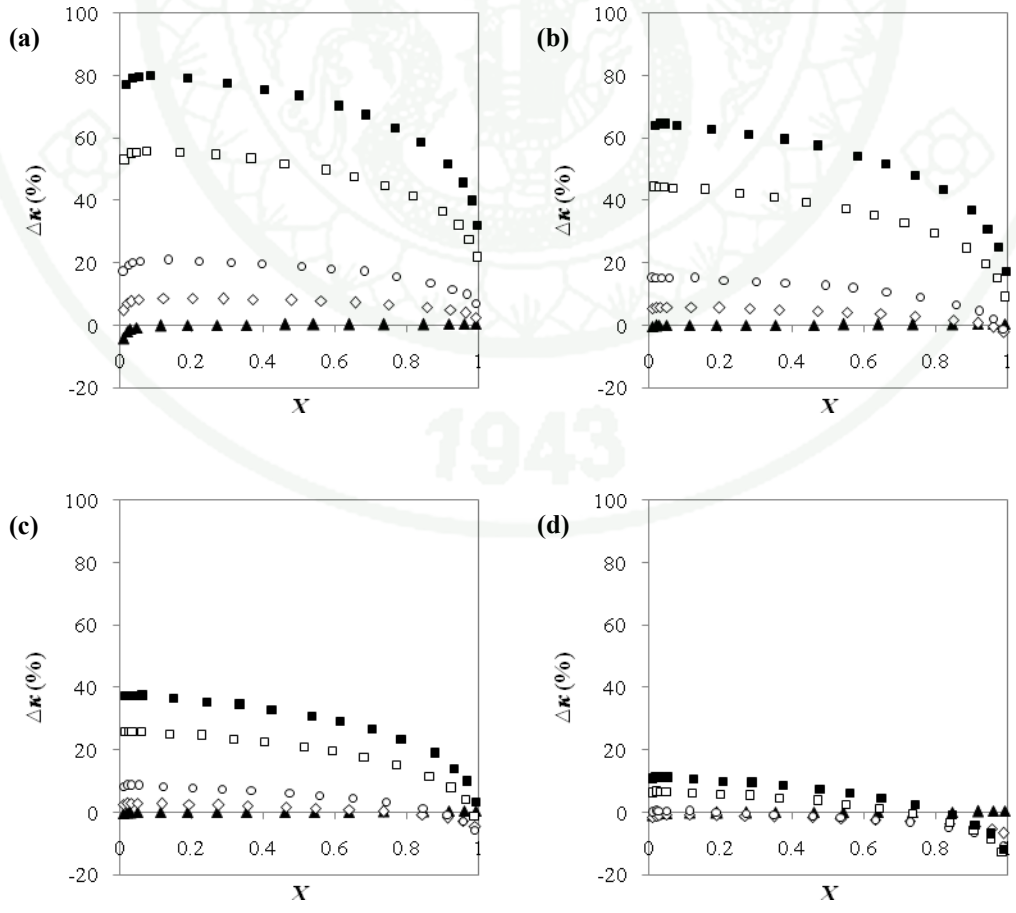

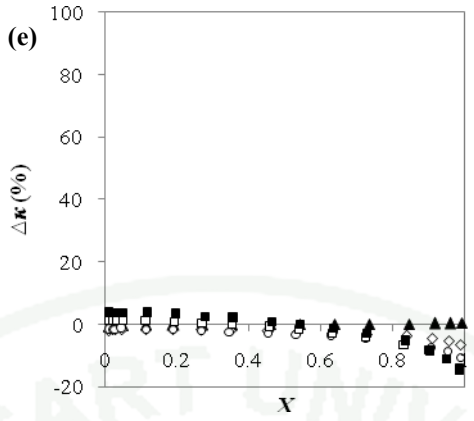

Figure 12 Plots of $\Delta\kappa$ (%) vs. conversion (X) for $T_{\xi=0.5}$ of 406 K (a), 498 K (b), 601 K (c), 705 K (d), and 810 K (e) at E = 1 kJ mol^{-1} (solid triangles), 25 kJ mol^{-1} (diamonds), 50 kJ mol^{-1} (circles), 100 kJ mol^{-1} (squares), and 125 kJ mol^{-1} (solid squares) for the conversion-expression-using method.

Figure 12 shows the plots of $\Delta\kappa$ (%) obtained from the conversion-expression-using method vs. conversion (X) for the reactor temperatures of 406, 498, 601, 705, and 810 K when the activation energy equals to 1, 25, 50, 100, and 125 kJ mol^{-1}. For $T_{\xi=0.5}$ of 406 K, the plot of $\Delta\kappa$ (%) at the conversions between 1 and 99% at different values of activation energy is shown in Figure 12(a). The significant change of quantities $\Delta\kappa$(%) with conversion is observed at E = 1 kJ mol^{-1} (solid triangles) in the conversion range between 1 and 11% but the change is considerably small compared with the curve fitting methods. $|\Delta\kappa(\%)|$ is approximately 0.1% at 11% conversion, smaller than that obtained at 1% conversion ($|\Delta\kappa(\%)|$ = 4.2%). The magnitudes of $|\Delta\kappa(\%)|$ at other conversions are small within which $|\Delta\kappa(\%)|$ does not exceed 0.5%. When E is increased, the increasing $|\Delta\kappa(\%)|$ with increasing activation energy according to Arrhenius equation is observed. The small change of $|\Delta\kappa(\%)|$ in the low conversions range is found at E = 25 (open diamonds), 50 (open circles), 100 (open squares), and 125 (solid squares) kJ mol^{-1}. The quantities $\Delta\kappa$ (%) at these activation energy values decrease with increasing conversion at the

conversion range between 11 and 99%. The significant change of $|\Delta\kappa(\%)|$ with conversion in the very high conversion range is also observed at E = 100 and 125 kJ mol^{-1}.

Figures 12(b) and 12(c) for $T_{\xi=0.5}$ of 498 and 601 K respectively show that $|\Delta\kappa(\%)|$ is comparably small throughout the range of conversions at E = 1 kJ mol^{-1}. When the activation energy is increased, $|\Delta\kappa(\%)|$ increases with increasing activation energy but decreases with increasing conversion. Similarly to Figure 12(a), the significant change of $|\Delta\kappa(\%)|$ with conversion in the very high conversions range is also obtained at E = 100 and 125 kJ mol^{-1}. The similar trend is observed in the plots of $\Delta\kappa$ (%) vs. conversion at different values of activation energy for $T_{\xi=0.5}$ of 705 and 810 K as shown in Figures 10(d) and 10(e) respectively. The conversion-expression-using method generally overestimates the reaction rate constants for $T_{\xi=0.5}$ of 406, 498, and 601 K. For $T_{\xi=0.5}$ of 705 K, the method can underestimate or overestimate the reaction rate constants depending on the magnitudes of conversion and activation energy. For $T_{\xi=0.5}$ of 810 K, the method generally provides the underestimated reaction rate constants except for very low activation energy values.

An advantage of the conversion-expression-using method is that it gives the information of the conversion which is the primary information related to the mass balance, prior to the reaction rate constants. However, when comparing the conversion-expression-using method with the two curve fitting methods, $\Delta\kappa$ (%) obtained from the conversion-expression-using method is generally slightly larger than those obtained from the exit-flow-rate-curve-fitting method but smaller than those obtained from the fitting of unit-area-normalized responses. These results suggest that the size of the response is an important characteristics that should be concerned in the quantitative interpretation.

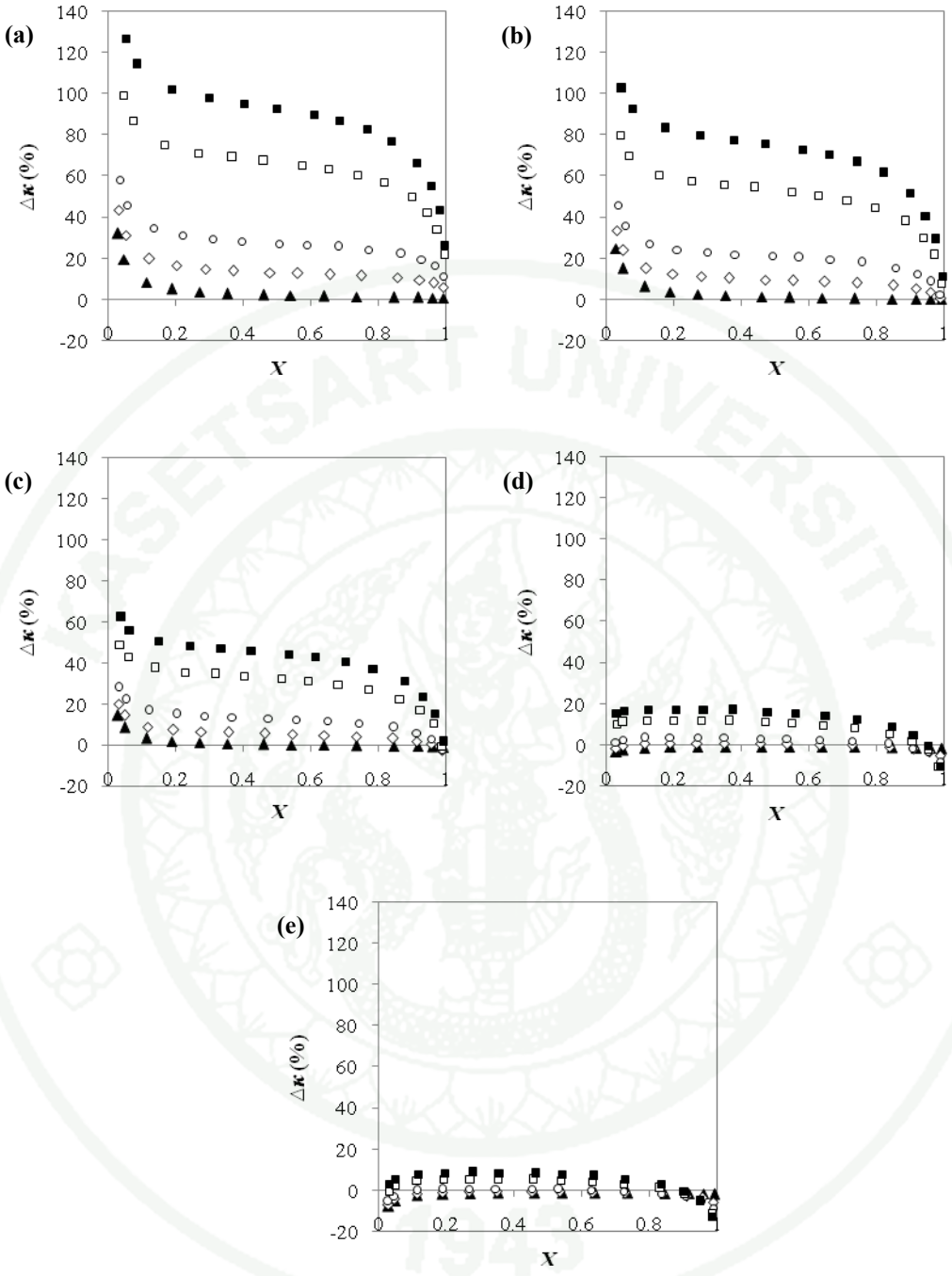

Figure 13 Plots of $\Delta\kappa$ (%) vs. conversion (X) for $T_{\xi=0.5}$ of 406 K (a), 498 K (b), 601 K (c), 705 K (d), and 810 K (e) at E = 1 kJ mol^{-1} (solid triangles), 25 kJ mol^{-1} (diamonds), 50 kJ mol^{-1} (circles), 100 kJ mol^{-1} (squares), and 125 kJ mol^{-1} (solid squares) for the mean-residence-time-expression-using method.

Figure 13 shows the plots of $\Delta\kappa$ (%) obtained from the mean-residence-time-expression-using method vs. conversion (X) for the reactor temperatures of 406, 498, 601, 705, and 810 K when the activation energy equals to 1, 25, 50, 100, and 125 kJ mol^{-1}. Figure 13(a) shows the plot of $\Delta\kappa$ (%) vs. conversion at different values of activation energy for $T_{\xi=0.5}$ of 406 K. At E = 1 kJ mol^{-1} (solid triangles), the quantities $\Delta\kappa(\%)$ change drastically with conversion at the conversion less than 20%. $|\Delta\kappa(\%)|$ at 11% conversion is approximately 5.1% which is much smaller than that at 3% conversion ($|\Delta\kappa(\%)|$ = 32.2%). The magnitudes of $|\Delta\kappa(\%)|$ obtained at other conversions are small within which $|\Delta\kappa(\%)|$ does not exceed 3%.

The magnitudes of $|\Delta\kappa(\%)|$ increase with increasing activation energy according to Arrhenius equation. At E = 25 (open diamonds), 50 (open circles), 100 (open squares), and 125 (solid squares) kJ mol^{-1}, the significant change of $|\Delta\kappa(\%)|$ with conversion is observed in the low conversions range. $\Delta\kappa$ (%) decreases with increasing conversion at the conversions between 20 and 99%. It is also found that the change of $|\Delta\kappa(\%)|$ with conversion is significant in the very high conversions range at high activation energy values of 100 and 125 kJ mol^{-1}. Similar plots of $\Delta\kappa$ (%) vs. conversion at different values of activation energy are obtained for $T_{\xi=0.5}$ of 498 and 601 K as shown in Figures 13(b) and 13(c) respectively.

Figures 13(d) and 13(e) for $T_{\xi=0.5}$ of 705 and 810 K respectively show that $|\Delta\kappa(\%)|$ is comparably small at E = 1 kJ mol^{-1} throughout the range of conversions. When the activation energy is increased, $|\Delta\kappa(\%)|$ increases with increasing activation energy but decreases with increasing conversion. The small change of $|\Delta\kappa(\%)|$ with conversion is also found at E = 50, 100, and 125 kJ mol^{-1}.

The mean-residence-time-expression-using method generally overestimates the reactant rate constants for all reactor temperatures and $|\Delta\kappa(\%)|$ obtained when using the mean-residence-time-expression-using method are considerably large

compared with other methods. It can be observed that the shape-concerning methods including the unit-area-normalized-response-fitting and the mean-residence-time-expression-using methods generally overestimate the reaction rate constants and give large $|\Delta\kappa(\%)|$. The results indicate that using only the shape of the response to determine the reaction rate constant may result in large errors of estimated parameters.

Among these four estimation methods, the exit-flow-rate-curve-fitting method should be apply to determine the reaction rate constants regarding to the good agreement between the simulated experimental and the model exit flow rate curves and the small deviations of the estimated reaction rate constants or small $|\Delta\kappa(\%)|$ compared with other methods. An advantage of the exit flow rate curve fitting method is that it concerns both the size and the shape of the response. However, in a real practice, the use of the exit flow rate to interpret the experimental data needs calibration by the use of an inert gas. The error caused by this calibration procedure is not included in the scope of this work. In addition, the deviation of estimated parameters may occur due to the signal noise (Roelant *et al.*, 2007) or the uncertainty of the injection pulse valve. The parameter deviation caused by these problems is also beyond the scope of this study.

According to Figures 10-13, it can be observed that the magnitudes of $|\Delta\kappa(\%)|$ decrease with increasing reactor temperature ($T_{\xi=0.5}$) for all estimation methods. Distributions of $\frac{\kappa(\xi)}{\kappa_{\xi=0.5}}$ along the axial coordinate of the reactor are investigated for different rector temperatures. As for the reaction rate constant, the relationship between the reaction rate constant and temperature follows the Arrhenius equation. At the same activation energy, the reaction rate constants at different reactor positions are calculated from the reaction rate constant at the middle position of the reactor using

$$\kappa(\xi) = \kappa_{\xi=0.5} \exp\left\{\frac{E}{R}\left(\frac{T(\xi)-T_{\xi=0.5}}{T(\xi)\times T_{\xi=0.5}}\right)\right\} \tag{44}$$

The distributions of $\frac{\kappa(\xi)}{\kappa_{\xi=0.5}}$ along the dimensionless reactor axial coordinate (ξ) for different reactor temperatures at $\kappa_{\xi=0.5}$ = 1.5 and E = 50 kJ mol^{-1} are shown in Figure 14. All the curves have equals to unity at the middle position of the reactor. In the first half of the reactor ($0 \leq \xi \leq 0.5$), the distribution of $\frac{\kappa(\xi)}{\kappa_{\xi=0.5}}$ is closer to unity for higher reactor temperatures. The distribution of $\frac{\kappa(\xi)}{\kappa_{\xi=0.5}}$ of the first half of the reactor probably affects the accuracy of estimated reaction rate constant in a greater extent than that in the second half of the reactor. As a result, a higher reactor temperature gives more accurate estimated reaction rate constant.

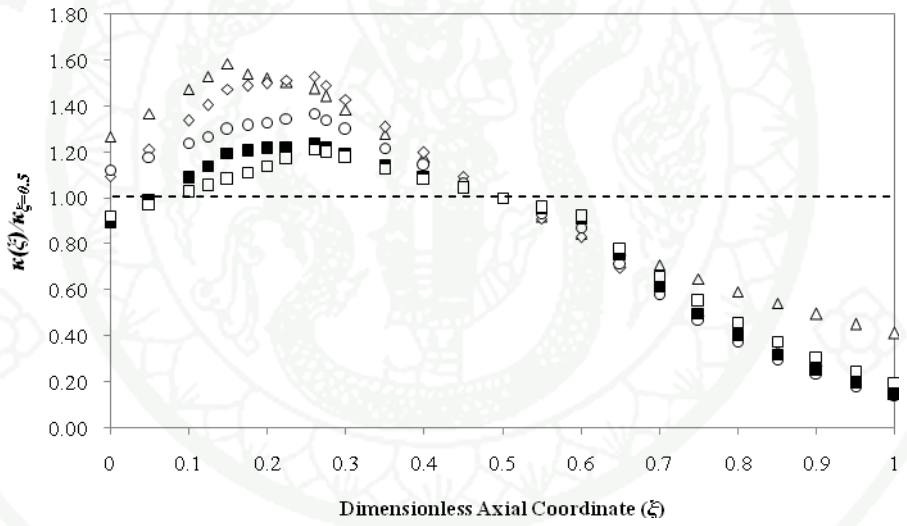

Figure 14 Distributions of $\frac{\kappa(\xi)}{\kappa_{\xi=0.5}}$ along the dimensionless axial coordinate (ξ) of the reactor for $T_{\xi=0.5}$ of 406 K (open triangles), 498 K (open diamonds), 601 K (open circles), 705 K (solid squares), and 810 K (open squares) at $\kappa_{\xi=0.5}$ = 1.5 and E = 50 kJ mol^{-1}.

CONCLUSIONS AND RECOMMENDATION

This study involves the analysis of the effect of non-uniform temperature distribution in a one-zone TAP microreactor on accuracy of estimated Knudsen gas diffusivities and estimated first order irreversible adsorption/reaction rate constants. Different methods are applied to estimate parameters from the TAP experimental response assuming uniform temperature distribution condition. The quantities ΔD_e and $\Delta\kappa$ are used to determine the accuracy of the estimated diffusivities and reaction rate constants, respectively. The same quantities can also indicate the validity of the uniform temperature distribution condition.

For the diffusion-only case, the quantities ΔD_e do not exceed 0.62% for both estimation methods including the exit-flow-rate-curve-fitting and the-mean-residence-time-expression-using methods. The results indicate that the uniform temperature distribution assumption is valid for estimation of diffusivities.

For the diffusion with first order irreversible adsorption/reaction case, all the estimation methods applied in this study give higher $|\Delta\kappa(\%)|$ than $|\Delta D_e(\%)|$ especially at low conversions. The quantities $\Delta\kappa$ (%) increase with increasing activation energy but decrease with increasing reactor temperature. The results obtained from this study suggest that the size of the experimental response should be involved in the quantitative interpretation procedure. In addition, the exit-flow-rate-curve-fitting method generally gives the smallest deviations of estimated reaction rate constants compared with other methods. The results also show that the validity of the uniform temperature distribution on estimation of rate constants depends on the estimation method and the uniform temperature distribution assumption is valid when the activation energy is low except for the low conversions range.

The results reported in this work are related to the one-zone reactor in which the total reactor is packed with inert or catalyst particles. In this case, the temperature gradient causes the rate constant to vary significantly along the reactor axial coordinate. Due to the strong dependence of the reaction rate constant on temperature

according to the Arrhenius equation, the magnitude of difference between the estimated the real reaction rate constants is very large and increases with the gradient of temperature. The scale of this gradient can be minimized by reducing the length of the catalyst bed, for example, in a thin-zone reactor configuration (Shekhtman et al., 1999) in which the thickness of the catalyst zone is made very small in comparison to the whole length of the reactor. In this case, the reaction rate constant can be assumed unvaried within the catalyst bed. However, the quantitative analysis of the effect of non-uniform temperature distribution on the accuracy of estimated gas diffusivities and reaction rate constants for other reactor configurations does not include in this study and will be investigated further.

For typical design of TAP reactor system, the reactor is placed between the pulse valve manifold and the vacuum chamber which are maintained at different temperatures. The reactor is normally wired with the heating wire with a uniform heating rate throughout the reactor. As a result, the temperature profile has a maximum inside the reactor. To obtain a more uniform temperature distribution, the reactor should be designed in such a way that the heating rate at the reactor inlet and outlet sections is higher. This may be achieved by a denser heater wiring in those sections.

LITERATURE CITED

Baerns, M., R. Imbihl, V.A. Kondratenko, R. Kraehnert, W.K. Offermans, R.A. Van Santen and A. Scheibe. 2005. Bridging the pressure and material gap in the catalytic ammonia oxidation: structural and catalytic properties of different platinum catalysts. **J. Catal.** 232: 226-238.

Breitkopf, C. 2005. A transient TAP study of the adsorption of C_4-hydrocarbons on sulfated zirconias. **J. Mol. Catal. A: Chem.** 226: 269-278.

Buyevskaya, O.V., K, Walter, D. Wolf and M. Baerns. 1996. Primary Reaction Steps and Active Surface Sites in the Rhodium-Catalyzed Partial Oxidation of Methane to CO and H_2. **Catal. Lett.** 38: 81-88.

Colaris, A.H.J., J. Hoebink, M. de Croon and J.C. Schouten. 2002. Intrapellet diffusivities from TAP pulse responses via moment-based analysis. **AIChE Journal** 48: 2587-2596.

Constales, D., S.O. Shekhtman, G.S. Yablonsky, G.B. Marin and J.T. Gleaves. 2006. Multi-zone TAP-reactors theory and application IV. Ideal and non-ideal boundary conditions. **Chem. Eng. Sci.** 61: 1878-1891.

Cunningham, R.E. and R.J.J. Williams. 1980. **Diffusion in Gases and Porous Media.** Plenum Press, New York.

Delgado, J.A., T.A. Nijhuis, F. Kapteijn and J.A. Moulijn. 2002. Modeling of fast pulse response in the Multitrack: an advanced TAP reactor. **Chem. Eng. Sci.** 57: 1835-1847.

_____, _____, _____ and _____. 2004. Determination of adsorption and diffusion parameters in zeolites through a structured approach. **Chem. Eng. Sci.** 59: 2477-2487.

Dewaele, O., D.Z. Wang and G.F. Froment. 1999. TAP Study of the sorption of H_2 and O_2 on Rh/γ-Al_20_3. **J. Mol. Catal. A: Chem.** 149: 263-273.

Fathi, M., A. Holmen, F. Monnet, Y. Schuurman and C. Mirodatos. 2000. Reactive oxygen species on platinum gauzes during partial oxidation of methane into synthesis gas. **J. Catal.** 190: 439-445.

Gleaves, J.T., J.R. Ebner and T.C., Kuechler. 1988. Temporal Analysis of Products (TAP) – A unique catalyst evaluation system with submillisecond time resolution. **Catal. Rev. Sci. Eng.** 30 (1): 49-116.

Gleaves, J.T., G.S. Yablonskii, P. Phanawadee and Y. Schuurman. 1997. TAP-2: An interrogative kinetics approach. **Appl. Catal. A: Gen** 160: 55-88.

Gleaves, J.T. 2001. Personal communication.

Gleaves, J.T., G.S. Yablonsky, X. Zheng, R. Fushimi and P. L. Mills. 2010. Temporal Analysis of Products (TAP) – Recent advances in technology for kinetic analysis of multicomponent catalysts. **J. Mol. Catal. A: Chem.** 315: 108-134.

Hanna, O.T. and O.C. Sandall. 1995. **Computational Methods in Chemical Engineering.** Prentice-Hall International, Inc., New York.

Heneghan, C.S., G.J. Hutchings, S.R. O'Leary, S.H. Taylor, V.J. Boyd and I.D. Hudson. 1999. A transient analysis of products study of the mechanism of VOC catalytic oxidation using uranium oxide catalysts. **Catal. Today** 54: 3-12.

Hindmarsh, A.C. 1972. **Linear Multistep Methods for Ordinary Differential Equations: Method Formulations, Stability, and the Methods of Nordsieck and Gear.** Lawrence Livermore Laboratory, University of California.

Huinink, J.P. 1995. **A Quantitative Analysis of Transient Kinetic Experiments: The Oxidation of CO by O_2/NO on Pt.** Ph.D. Thesis, Eindhoven University of Technology, Eindhoven, The Netherlands.

Huizenga, D.G. and D.M. Smith. 1986. Knudsen diffusion in random assemblages of uniform spheres. **AIChE Journal** 32: 1-6.

Kondratenko, E.V. and J. Pérez-Ramírez. 2004. Oxidative functionalization of propane over FeMFI zeolites: Effect of reaction variables and catalyst constitution on the mechanism and performance. **Appl. Catal. A** 267: 181-189.

Kondratenko, E.V., M. Cherian and M. Baerns. 2005. Mechanistic aspects of the oxidative dehydrogenation of propane over an alumina-supported $VCrMnWO_x$ mixed oxide catalyst. **Catal. Today** 99: 59-67.

Konietzni, F., H.W. Zanthoff and W.F. Maier. 1999. The role of active oxygen in the AMM-VxSi-catalysed selective oxidation of toluene. **J. Catal.** 188: 154-164.

Kreyzig, E. 1993. **Advanced Engineering Mathematics.** 7th ed., John Wiley and Sons, Inc., Singapore.

Mason, E.A., R.B. Evans and G.M. Watson. 1963. Gaseous diffusion in porous media. III. Thermal Transpiration. **Journal of Chemical Physics** 38 (8): 1808-1826.

Mason, E.A., A.P. Malinauskas and R.B. Evans. 1967. Flow and diffusion of gases in porous media. **Journal of Chemical Physics** 46 (8): 3199-3216.

Nijhuis, T.A., L.J.P. Van Den Broeke, M.J.G. Linders, M. Makkee, F. Kapteijn and J.A. Moulijn. 1999. Modeling of the transient sorption and diffusion processes in microporous materials at low pressure. **Catal. Today** 53: 189-205.

Olea, M., M. Florea, I. Sack, R.P. Silvy, E.M. Gaigneaux, G.B. Marin and P. Grange. 2005. Evidence for the participation of lattice nitrogen from vanadium aluminum oxynitrides in propane ammoxidation. **J. Catal.** 232: 152-160.

Petzold, L.R. 1983. Automatic selection of methods for solving stiff and nonstiff systems of ordinary differential equations. **Siam J. Sci. Stat. Comput.** 4: 136-148.

Pérez-Ramírez, J., E.V. Kondratenko, V.A. Kondratenko and M. Baerns. 2004. Selectivity-directing factors of ammonia oxidation over PGM gauzes in the Temporal Analysis of Products reactor : Primary interactions of NH_3 and O_2. **J. Catal.** 227: 90-100.

_____, _____, _____ and _____. 2005. Selectivity-directing factors of ammonia oxidation over PGM gauzes in the Temporal Analysis of Products reactor : Secondary interactions of NH_3 and NO. **J. Catal.** 229: 303-313.

Pérez-Ramírez, J. and E.V. Kondratenko. 2007. Evolution, achievements, and perspectives of the TAP technique. **Catal. Today** 121: 160-169.

Phanawadee, P. 1997. **Theory and Methodology of TAP Knudsen Pulse Response Experiments.** Ph.D. Thesis, Washington University, Saint Louis, Missouri, USA.

Phanawadee, P., S.O. Shekhtman, C. Jarungmanorom, G.S. Yablonsky and J.T. Gleaves. 2003. Uniformity in a thin-zone multi-pulse TAP experiment: numerical analysis. **Ind. Eng. Chem. Res.** 38: 2877-2878.

Roelant, R., D. Constales, G.S. Yablonsky, R. Van Keer, M.A. Rude and G.B. Marin. 2007. Noise in temporal analysis of products (TAP) pulse responses. **Catal. Today** 121: 269-281.

Rodemerck, U., B. Kubias, H.W. Zanthoff and M. Baerns. 1997. The reaction mechanism of the selective oxidation of butane on $(VO)_2P_2O_7$ catalysts: The role of oxygen in the reaction chain to maleic anhydride. **Appl. Catal. A** 153: 203-216.

Schuurman, Y., A. Pantazidis and C. Mirodatos. 1999. The TAP-2 reactor as an alternative tool for investigating FCC catalyst. **Chem. Eng. Sci.** 54: 3619- 3625.

Shekhtman, S.O., G.S. Yablonsky, S. Chen and J.T. Gleaves. 1999. Thin-zone TAP-reactor-theory and application. **Chem. Eng. Sci.** 54: 4371-4378.

Svoboda, G.D. 1993. **Fundamental transport-kinetic models for interpretation of TAP reactor transient response data with application to reactive systems.** Ph.D. Dissertation, Washington University, Saint Louis, Missouri, USA.

Tantake, P., P. Phanawadee, Y. Boonnumpha and J. Limtrakul. 2007. Comparison between regression analysis and moment analysis for transport and kinetic parameter estimation in TAP experiments under a non-ideal inlet condition. **Catal. Today** 121: 261-268.

Wang D.Z., O. Dewaele and G.F. Froment. 1998. Methane adsorption on Rh/Al_2O_3. **J. Mol. Catal. A: Chem.** 136: 301-309.

Zou, B., M.P. Dudukovic and P.L. Mills. 1993. Modelling of evacuated pulse micro-reactor. **Chem. Eng. Sci.** 48: 2345-2355.

APPENDICES

Appendix A

Discretization of the Mathematical Model for Diffusion with First Order Irreversible Adsorption/Reaction in a One-Zone Reactor Under Non-Uniform Temperature Distribution Condition

In this study, the set of PDEs describing the transport and kinetic processes in a one-zone TAP reactor under the non-uniform temperature distribution condition is numerically solved using the so-called Method of Lines (MOL). The method of lines is an important numerical procedure for the solution of evolutionary partial differential equations (PDEs). The idea is to discretize the partial derivatives with respect to all independent variables except the time variable which remains continuous. This process leads to a system of ordinary differential equations (ODEs) for the discretized variables which can then, in principle, be solved by the initial value method. The discretization of MOL can be accomplished using the method of finite differences.

According to the Taylor's expansion, we can write

$$\phi(\xi_{i+1},\tau) = \phi(\xi_i,\tau) + h_\xi \frac{\partial\phi(\xi_i,\tau)}{\partial\xi} + \frac{h_\xi^2}{2!}\frac{\partial^2\phi(\xi_i,\tau)}{\partial\xi^2} + \cdots \quad \text{A-1}$$

$$\phi(\xi_{i-1},\tau) = \phi(\xi_i,\tau) - h_\xi \frac{\partial\phi(\xi_i,\tau)}{\partial\xi} + \frac{h_\xi^2}{2!}\frac{\partial^2\phi(\xi_i,\tau)}{\partial\xi^2} - \cdots \quad \text{A-2}$$

From the Taylor's series written in Eqs. (A-1) and (A-2), the central finite difference approximation for the second order derivative is described by

$$\left(\frac{\partial^2\phi(\tau)}{\partial\xi^2}\right)_i = \frac{\phi_{i+1}(\tau) - 2\phi_i(\tau) + \phi_{i-1}(\tau)}{h_\xi^2} - \frac{h_\xi^2}{12}\left(\frac{\partial^4\phi(\tau)}{\partial\xi^4}\right)_i + \cdots$$

or,
$$\left(\frac{\partial^2\phi(\tau)}{\partial\xi^2}\right)_i \cong \frac{\phi_{i+1}(\tau) - 2\phi_i(\tau) + \phi_{i-1}(\tau)}{h_\xi^2} \quad \text{A-3}$$

The central finite difference approximation for first order derivative is given by

$$\left(\frac{\partial\phi(\tau)}{\partial\xi}\right)_i = \frac{\phi_{i+1}(\tau) - \phi_{i-1}(\tau)}{2h_\xi} + \frac{h_\xi^2}{6}\left(\frac{\partial^3\phi(\tau)}{\partial\xi^3}\right)_i + \cdots$$

or,
$$\left(\frac{\partial\phi(\tau)}{\partial\xi}\right)_i \cong \frac{\phi_{i+1}(\tau)-\phi_{i-1}(\tau)}{2h_\xi} \qquad \text{A-4}$$

According to Eq. (A-1), the forward finite difference approximation for the first order derivative is described by

$$\left(\frac{\partial\phi(\tau)}{\partial\xi}\right)_i = \frac{-\phi_{i+2}(\tau)+4\phi_{i+1}(\tau)-3\phi_i(\tau)}{2h_\xi} + \frac{h_\xi^2}{6}\left(\frac{\partial^3\phi(\tau)}{\partial\xi^3}\right)_i + \cdots$$

or,
$$\left(\frac{\partial\phi(\tau)}{\partial\xi}\right)_i \cong \frac{-\phi_{i+2}(\tau)+4\phi_{i+1}(\tau)-3\phi_i(\tau)}{2h_\xi} \qquad \text{A-5}$$

According to Eq. (A-2), the backward finite difference approximation for first order derivative is given by

$$\left(\frac{\partial\phi(\tau)}{\partial\xi}\right)_i = \frac{3\phi_i(\tau)-4\phi_{i-1}(\tau)+\phi_{i-2}(\tau)}{2h_\xi} - \frac{h_\xi^2}{6}\left(\frac{\partial^3\phi(\tau)}{\partial\xi^3}\right)_i + \cdots$$

or,
$$\left(\frac{\partial\phi(\tau)}{\partial\xi}\right)_i \cong \frac{3\phi_i(\tau)-4\phi_{i-1}(\tau)+\phi_{i-2}(\tau)}{2h_\xi} \qquad \text{A-6}$$

where h_ξ is the step size between the axial coordinate of the reactor.

The mass balance equation for diffusion with first order irreversible adsorption/reaction in a one-zone reactor under non-uniform temperature distribution condition is described in the generalized dimensionless form as

$$\frac{\partial C^*(\tau,\xi)}{\partial\tau} = \left\{\frac{\partial}{\partial\xi}\left(\frac{D_e(\xi)}{D_{e,\xi=0.5}}\frac{\partial C^*(\tau,\xi)}{\partial\xi}\right) + \frac{1}{2}\frac{\partial}{\partial\xi}\left(\frac{D_e(\xi)}{D_{e,\xi=0.5}}C^*(\tau,\xi)\frac{\partial\ln T(\xi)}{\partial\xi}\right)\right\}$$
$$-r_\kappa\kappa_{\xi=0.5}C^*(\tau,\xi) \qquad \text{A-7}$$

or,

$$\frac{\partial C^*(\tau,\xi)}{\partial \tau} = \frac{1}{2}\left\{\left(r_D C^*(\tau,\xi)\frac{1}{T(\xi)}\frac{\partial^2 T(\xi)}{\partial \xi^2} \right.\right.$$

$$+\frac{\partial T(\xi)}{\partial \xi}\left[r_D\left(\frac{1}{T(\xi)}\frac{\partial C^*(\tau,\xi)}{\partial \xi} - C^*(\tau,\xi)\frac{1}{T^2(\xi)}\frac{\partial T(\xi)}{\partial \xi} \right) + C^*(\tau,\xi)\frac{1}{T(\xi)}\frac{\partial r_D}{\partial \xi} \right]\Bigg)$$

$$\left. +r_D\frac{\partial^2 C^*(\tau,\xi)}{\partial \xi^2} + \frac{\partial C^*(\tau,\xi)}{\partial \xi}\frac{\partial r_D}{\partial \xi} \right\} - r_\kappa \kappa_{\xi=0.5} C^*(\tau,\xi) \qquad \text{A-8}$$

where
$$r_\kappa = \frac{D_e(\xi)}{D_{e,\xi=0.5}} \qquad \text{A-9}$$

$$r_\kappa = \frac{\kappa(\xi)}{\kappa_{\xi=0.5}} \exp\left\{ \frac{E}{R}\left(\frac{T(\xi)-T_{\xi=0.5}}{T(\xi)\times T_{\xi=0.5}} \right) \right\} \qquad \text{A-10}$$

The dimensionless initial and boundary conditions are described by

$$\tau = 0; \qquad C^*(\tau,\xi) = \delta(\xi - 0^+) \qquad \text{A-11}$$

$$\xi = 0; \qquad \frac{\partial C^*(\tau,\xi)}{\partial \xi} = 0 \qquad \text{A-12}$$

$$\xi = 1; \qquad C^*(\tau,\xi) = 0 \qquad \text{A-13}$$

The dimensionless exit flow rate of the gas is calculated using

$$F^*(\tau,\xi) = -\left\{ r_D\left(\frac{\partial C^*(\tau,\xi)}{\partial \xi} + \frac{1}{2}C^*(\tau,\xi)\frac{\partial \ln T(\xi)}{\partial \xi} \right) \right\}\Bigg|_{\xi=1} \qquad \text{A-14}$$

The mass balance equation described by Eq. (A-8) is transformed into the first order ordinary differential equation with respect to time using the central finite approximation for first and second order derivatives. The discretization along the axial coordinate of the reactor is written as

$$\left(\frac{dC^*}{d\tau}\right)_i = \frac{1}{2}\left\{\left(r_D C_i^* \frac{1}{T_i}\left(\frac{(T_{i+1} - 2T_i + T_{i-1})}{h_\xi^2} \right) \right.\right.$$

$$\left.\left. +\left(\frac{T_{i+1} - T_{i-1}}{2h_\xi} \right)\left[r_D\left(\frac{1}{T_i}\left(\frac{C_{i+1}^* - C_{i-1}^*}{2h_\xi} \right) - C_i^*\frac{1}{T_i^2}\left(\frac{T_{i+1} - T_{i-1}}{2h_\xi} \right) \right) + C_i^*\frac{1}{T_i}\left(\frac{r_{D,i+1} - r_{D,i-1}}{2h_\xi} \right) \right] \right)\right.$$

$$+r_D\left(\frac{C^*_{i+1}-2C^*_i+C^*_{i-1}}{h^2_\xi}\right)+\left(\frac{C^*_{i+1}-C^*_{i-1}}{2h_\xi}\right)\left(\frac{r_{D,i+1}-r_{D,i-1}}{2h_\xi}\right)\Bigg\}-r_\kappa\kappa_{\xi=0.5}C^*_i \qquad \text{A-15}$$

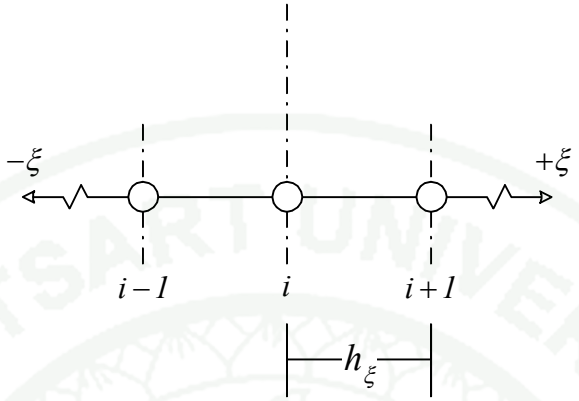

Appendix Figure A1 Discretization along the axial coordinate of the reactor.

The initial value specifies in Eq. (A-11) explains that the N_P moles of gas is injected into the reactor at $t=0$ and the corresponding gas concentration in the inlet pulse can be represented by the Dirac delta function placed at $z=0^+$. The definition of Delta function is described by (Kreyszig, 1993)

$$\int_0^1 C^* d\xi = \int_{-\infty}^{+\infty} \delta(\xi-0^+)d\xi \equiv 1 \qquad \text{A-16}$$

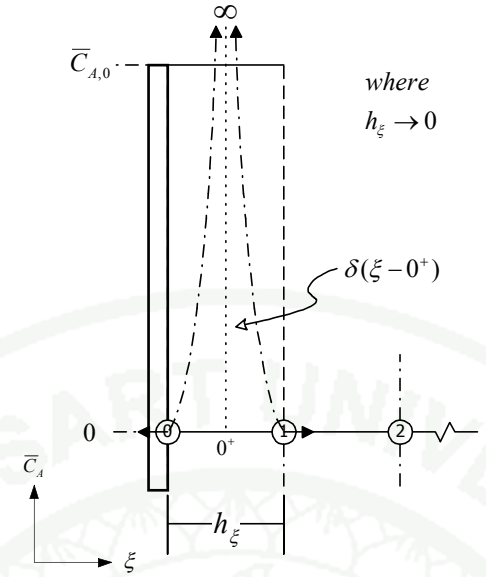

Appendix Figure A2 Discretization at the reactor inlet and the Delta function.

According to the definition, when the concentration at the first and the next reactor axial coordinates is set to be the same, the integral equation can be described the area of rectangular which is $C_0^*(\tau = 0)$ in height and h_ξ in width (see Appendix Figure 2) and the gas concentrations at other reactor axial coordinates are zero. Consequently, we obtain the set of equations describing the initial condition written as

$$C_i^*(\tau = 0) = \begin{cases} \dfrac{1}{h_\xi} & \text{for} \quad 0 \le \xi_i \le h_\xi \\ 0 & \text{for} \quad h_\xi < \xi_i \le 1 \end{cases} \qquad \text{A-17}$$

The inlet boundary condition given by Eq. (A-12) corresponds to the absence of flux at the reactor entrance when the pulse valve is closed. The outlet boundary condition given by Eq. (A-13) specifies that the reactor outlet is held at vacuum conditions and therefore the gas concentration is zero. The PDEs describe the boundary condition at the reactor inlet and outlet are called the Neumann boundary condition and the Dirichlet boundary condition, respectively. These two boundary conditions at the inlet and outlet of the reactor are discretized as follows:

At the reactor inlet; $$\left(\frac{\partial C^*}{\partial \xi}\right)_{i=0} = \frac{C_1^* - C_0^*}{h_\xi} = 0 \quad \text{A-18}$$

hence, we obtain $$\left(\frac{dC^*}{d\tau}\right)_{i=0} = \left(\frac{dC^*}{d\tau}\right)_{i=1} \quad \text{A-19}$$

The gas concentration is zero at the reactor outlet, therefore

$$\left(\frac{dC^*}{d\tau}\right)_{i=outlet} = 0 \quad \text{A-20}$$

The first order PDE describing the exit flow rate of the gas in Eq. (A-14) can be discretized using the backward finite approximation. Is it noted that due to the zero gas concentration at the reactor exit, Eq. (A-14) can be rewritten as

$$F^*(\tau,\xi) = -\left(\frac{\partial C^*(\tau,\xi)}{\partial \xi}\right)\Bigg|_{\xi=1} \quad \text{A-21}$$

Eq. (A-21) is then discretized as follows:

$$F^* = -r_{D,i}\left(\frac{3C_i^* - 4C_{i-1}^* + C_{i-2}^*}{2h_\xi}\right) = r_{D,i}\left(\frac{4C_{i-1}^* - C_{i-2}^*}{2h_\xi}\right) \quad \text{A-22}$$

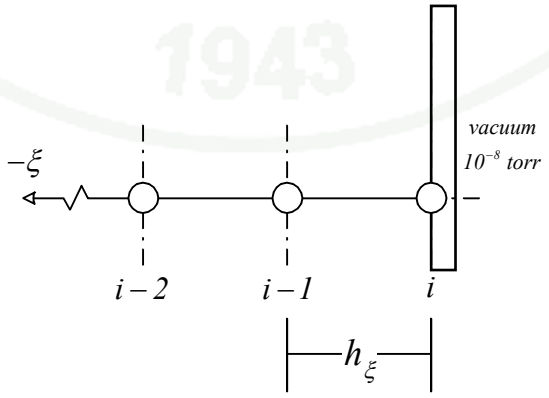

Appendix Figure A3 Discretization at the reactor exit.

Appendix B

TAP Reactor Temperature Gradient Experiment Description

An insert was fabricated to fit the exit of the TAP reactor to enable the placement of glass capillary tubes holding thermocouple leads:

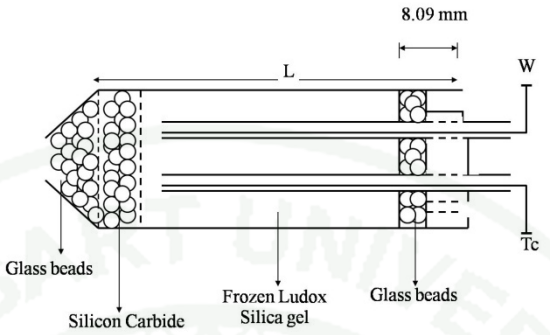

Appendix Figure B1 A schematic of the TAP-1 reactor configuration used in the temperature gradient experiment.

The reactor was packed with glass beads, silicon carbide and silica gel particles to simulate a packed reactor. The 0.124-0.125 g of glass beads (590-894 mesh, 0.357 g of frozen Ludox silica gel (75-50 mesh), and 0.10 g of glass beads (590-840 mesh) were packed.

The thermocouple wells and thermocouples were placed in the reactor prior to adding the silica gel. The thermocouples were held in place within the glass thermocouple wells by a kink in each wire. The glass thermocouple wells themselves were held in place by the friction of the insert and the bed. The temperature reading were designated T_w (for the out well) and T_c (for the center well).

The reactor was set in place and evacuated to ca. 10^{-7} torr with the thermocouple wells placed at deepest locations near the beginning of the silica gel packing. All of the required temperature readings were taken at these initial thermocouple well positions. The reactor was then cooled down and the wells replaced and the procedure repeated until five lateral positions had been measured. The temperatures measured at different reactor positions in the presence of a pulsing gas are reported in Appendix Table B1.

Appendix Table B1 Actual temperature values measured at different reactor positions with inert gas pulsing.

Control Temperature, ° C	Reactor Temperature, ° C	Side Temperature[a], ° C	Axial Temperature[b], ° C	TC LOC.[c], mm	FRAC LOC., from reactor entrance
150	144.8	128.8	126.8	10.74	0.741
150	145.8	136.8	134.8	16.24	0.609
150	145.8	143.8	143.8	26.24	0.368
150	146.8	148.8	146.8	30.74	0.259
150	146.8	140.8	144.8	35.51	0.144
150		139.8	139.8	38.30	0.077
250	247.8	214.8	210.8	10.74	0.741
250	243.8	231.8	229.8	16.24	0.609
250	243.8	241.8	241.8	26.24	0.368
250	244.8	248.8	247.8	30.74	0.259
250	245.8	238.8	242.8	35.51	0.144
250		234.8	233.8	38.30	0.077
350	346.8	305.8	301.8	10.74	0.741
350	344.8	332.8	330.8	16.24	0.609
350	347.8	345.8	346.8	26.24	0.368
350	344.8	351.8	350.8	30.74	0.259
350	346.8	340.8	346.8	35.51	0.144
350		334.8	332.8	38.30	0.077
450	448.8	398.8	394.8	10.74	0.741
450	444.8	431.8	430.8	16.24	0.609
450	444.8	446.8	449.8	26.24	0.368
450	446.8	455.8	454.8	30.74	0.259
450	447.8	440.8	447.8	35.51	0.144
450		434.8	432.8	38.30	0.077

Appendix Table B1 (Continued)

Control Temperature, ° C	Reactor Temperature, ° C	Side Temperature[a], ° C	Axial Temperature[b], ° C	TC LOC.[c], mm	FRAC LOC., from reactor entrance
550	549.8	489.8	486.8	10.74	0.741
550	546.8	532.8	532.8	16.24	0.609
550	546.8	550.8	552.8	26.24	0.368
550	547.8	559.8	558.8	30.74	0.259
550	547.8	539.8	545.8	35.51	0.144
550		536.8	534.8	38.3	0.077

[a] Side Temperature is measured 1.0 mm from the reactor wall, [b] Axial Temperature is measured (2.5 mm from wall) along the axis of the reactor, [c] TC LOC is the position of the thermocouple measured from the reactor exit (in mm), temperatures are corrected for differences in thermocouple readings

Sources: Gleaves, J.T. (2001)

Appendix C

Simulated Results for κ_{est} and $\Delta\kappa$ (%) Obtained from the Exit-Flow-Rate-Curve-Fitting Method at Various $\kappa_{\xi=0.5}$ and E for Different $T_{\xi=0.5}$

Appendix Table C1 Simulated results for κ_{est} and $\Delta\kappa$ (%) obtained from the exit-flow-rate-curve-fitting method at various $\kappa_{\xi=0.5}$ and E for different $T_{\xi=0.5}$.

$\kappa_{\xi=0.5}$	$T_{\xi=0.5}$ (K)	E = 1 (kJ mol^{-1})		E = 25 (kJ mol^{-1})		E = 50 (kJ mol^{-1})		E = 100 (kJ mol^{-1})		E = 125 (kJ mol^{-1})	
		κ_{est}	$\Delta\kappa$ (%)	κ_{est}	$\Delta\kappa$ (%)	κ_{est}	$\Delta\kappa$ (%)	κ_{est}	$\Delta\kappa$ (%)	κ_{est}	$\Delta\kappa$ (%)
0.02	406	0.016596	-17.0192	0.018322	-8.3916	0.020724	3.6179	0.027688	38.4383	0.032480	62.4015
	498	0.015557	-22.2147	0.016645	-16.7765	0.018471	-7.6454	0.024133	20.6649	0.028052	40.2616
	601	0.014903	-25.4851	0.015415	-22.9229	0.016483	-17.5830	0.019865	-0.6770	0.022116	10.5790
	705	0.014759	-26.2050	0.014593	-27.0330	0.014800	-25.9981	0.015966	-20.1699	0.016827	-15.8639
	810	0.015041	-24.7938	0.014749	-26.2552	0.014726	-26.3720	0.015244	-23.7789	0.015706	-21.4685
0.04	406	0.036597	-8.5069	0.040040	0.1001	0.044833	12.0814	0.058723	46.8082	0.068277	70.6931
	498	0.035486	-11.2849	0.037651	-5.8721	0.041292	3.2304	0.052584	31.4609	0.060398	50.9957
	601	0.034795	-13.0137	0.035810	-10.4744	0.037938	-5.1561	0.044681	11.7022	0.049171	22.9273
	705	0.034625	-13.4385	0.034286	-14.2852	0.034694	-13.2653	0.037015	-7.4628	0.038732	-3.1699
	810	0.034910	-12.7257	0.034319	-14.2028	0.034267	-14.3322	0.035296	-11.7591	0.036217	-9.4577

Appendix Table C1 (Continued)

$\kappa_{\zeta=0.5}$	$T_{\zeta=0.5}$ (K)	E = 1 (kJ mol^{-1})		E = 25 (kJ mol^{-1})		E = 50 (kJ mol^{-1})		E = 100 (kJ mol^{-1})		E = 125 (kJ mol^{-1})	
		κ_{est}	$\Delta\kappa$ (%)	κ_{est}	$\Delta\kappa$ (%)	κ_{est}	$\Delta\kappa$ (%)	κ_{est}	$\Delta\kappa$ (%)	κ_{est}	$\Delta\kappa$ (%)
0.06	406	0.056599	-5.6690	0.061750	2.9173	0.068922	14.8706	0.089703	49.5048	0.103987	73.3123
	498	0.055415	-7.6409	0.058648	-2.2534	0.064093	6.8209	0.080983	34.9718	0.092667	54.4457
	601	0.054687	-8.8555	0.056197	-6.3390	0.059375	-1.0421	0.069461	15.7685	0.076178	26.9635
	705	0.054491	-9.1818	0.053972	-10.0471	0.054575	-9.0422	0.058041	-3.2652	0.060609	1.0147
	810	0.054779	-8.7018	0.053883	-10.1946	0.053798	-10.3365	0.055330	-7.7832	0.056705	-5.4908
0.1	406	0.096602	-3.3980	0.105147	5.1474	0.117045	17.0453	0.151497	51.4967	0.175152	75.1519
	498	0.095276	-4.7240	0.100613	0.6130	0.109631	9.6312	0.137625	37.6253	0.156979	56.9792
	601	0.094473	-5.5271	0.096944	-3.0557	0.102199	2.1987	0.118915	18.9153	0.130050	30.0497
	705	0.094226	-5.7743	0.093323	-6.6767	0.094299	-5.7015	0.100025	0.0251	0.104279	4.2791
	810	0.094520	-5.4805	0.092995	-7.0046	0.092829	-7.1713	0.095343	-4.6571	0.097617	-2.3828
0.25	406	0.246623	-1.3507	0.267612	7.0448	0.296851	18.7404	0.381336	52.5343	0.439122	75.6488
	498	0.244770	-2.0919	0.257651	3.0604	0.279685	11.8741	0.348257	39.3029	0.395572	58.2287
	601	0.243694	-2.5223	0.249458	-0.2170	0.262205	4.8820	0.303142	21.2567	0.330438	32.1753
	705	0.243256	-2.6977	0.240660	-3.7361	0.242826	-2.8697	0.256681	2.6723	0.267082	6.8329
	810	0.243572	-2.5712	0.239475	-4.2102	0.238830	-4.4679	0.244757	-2.0970	0.250281	0.1122

Appendix Table C1 (Continued)

$\kappa_{\xi=0.5}$	$T_{\xi=0.5}$ (K)	E = 1 (kJ mol^{-1})		E = 25 (kJ mol^{-1})		E = 50 (kJ mol^{-1})		E = 100 (kJ mol^{-1})		E = 125 (kJ mol^{-1})	
		κ_{est}	$\Delta\kappa$ (%)	κ_{est}	$\Delta\kappa$ (%)	κ_{est}	$\Delta\kappa$ (%)	κ_{est}	$\Delta\kappa$ (%)	κ_{est}	$\Delta\kappa$ (%)
0.45	406	0.446672	-0.7395	0.483590	7.4644	0.535070	18.9044	0.683478	51.8841	0.784549	74.3442
	498	0.444138	-1.3026	0.466259	3.6131	0.504753	12.1674	0.625025	38.8943	0.707845	57.2988
	601	0.442710	-1.6199	0.452127	0.4726	0.474182	5.3739	0.545940	21.3199	0.593870	31.9711
	705	0.442022	-1.7728	0.436563	-2.9861	0.439836	-2.2588	0.463720	3.0490	0.481914	7.0921
	810	0.442370	-1.6956	0.434330	-3.4822	0.432645	-3.8566	0.442492	-1.6684	0.452060	0.4578
0.7	406	0.696767	-0.4619	0.752601	7.5145	0.830590	18.6557	1.054951	50.7073	1.207085	72.4407
	498	0.693415	-0.9408	0.725858	3.6941	0.783611	11.9444	0.965072	37.8675	1.089823	55.6890
	601	0.691566	-1.2049	0.704440	0.6343	0.737118	5.3026	0.845264	20.7520	0.917691	31.0987
	705	0.690574	-1.3466	0.680621	-2.7684	0.684557	-2.2061	0.719785	2.8264	0.747129	6.7328
	810	0.690961	-1.2912	0.677222	-3.2540	0.673630	-3.7671	0.687438	-1.7946	0.701642	0.2346
1	406	0.996926	-0.3074	1.074131	7.4131	1.182226	18.2226	1.492736	49.2736	1.702458	70.2458
	498	0.992639	-0.7361	1.035818	3.5818	1.114942	11.4942	1.365462	36.5462	1.537524	53.7524
	601	0.990311	-0.9689	1.005838	0.5838	1.049913	4.9913	1.198955	19.8955	1.299142	29.9142
	705	0.988965	-1.1035	0.972383	-2.7617	0.976144	-2.3856	1.023399	2.3399	1.060956	6.0956
	810	0.989403	-1.0597	0.967778	-3.2222	0.961078	-3.8922	0.978384	-2.1616	0.997595	-0.2405

Appendix Table C1 (Continued)

$\kappa_{\zeta=0.5}$	$T_{\zeta=0.5}$ (K)	E = 1 (kJ mol^{-1})		E = 25 (kJ mol^{-1})		E = 50 (kJ mol^{-1})		E = 100 (kJ mol^{-1})		E = 125 (kJ mol^{-1})	
		κ_{est}	$\Delta\kappa$ (%)	κ_{est}	$\Delta\kappa$ (%)	κ_{est}	$\Delta\kappa$ (%)	κ_{est}	$\Delta\kappa$ (%)	κ_{est}	$\Delta\kappa$ (%)
1.5	406	1.497296	-0.1802	1.607245	7.1497	1.761961	17.4641	2.206079	47.0719	2.504782	66.9855
	498	1.491558	-0.5628	1.549057	3.2705	1.660137	10.6758	2.016957	34.4638	2.262081	50.8054
	601	1.488490	-0.7673	1.505187	0.3458	1.565381	4.3588	1.776878	18.4585	1.920073	28.0049
	705	1.486576	-0.8949	1.456247	-2.9169	1.457625	-2.8250	1.521567	1.4378	1.574544	4.9696
	810	1.487103	-0.8598	1.450050	-3.3300	1.436391	-4.2406	1.456842	-2.8772	1.483229	-1.1181
2	406	1.997788	-0.1106	2.137373	6.8687	2.334954	16.7477	2.902686	45.1343	3.283640	64.1820
	498	1.990717	-0.4642	2.058649	2.9325	2.197799	9.8899	2.652019	32.6009	2.964625	48.2312
	601	1.986975	-0.6512	2.001294	0.0647	2.074508	3.7254	2.342546	17.1273	2.525493	26.2747
	705	1.984521	-0.7739	1.937476	-3.1262	1.934181	-3.2910	2.011227	0.5614	2.077960	3.8980
	810	1.985139	-0.7430	1.930144	-3.4928	1.907572	-4.6214	1.928252	-3.5874	1.960596	-1.9702
2.8	406	2.798797	-0.0430	2.980431	6.4439	3.240317	15.7256	3.990026	42.5009	4.492550	60.4482
	498	2.789810	-0.3639	2.867681	2.4172	3.045182	8.7565	3.641012	30.0361	4.053127	44.7545
	601	2.785111	-0.5317	2.789382	-0.3792	2.878155	2.7913	3.226935	15.2477	3.468353	23.8698
	705	2.781838	-0.6486	2.702828	-3.4704	2.688062	-3.9978	2.779984	-0.7149	2.865956	2.3556
	810	2.782608	-0.6211	2.694484	-3.7684	2.654248	-5.2054	2.670282	-4.6328	2.710002	-3.2142

Appendix Table C1 (Continued)

$\kappa_{\xi=0.5}$	$T_{\xi=0.5}$ (K)	E = 1 (kJ mol^{-1})		E = 25 (kJ mol^{-1})		E = 50 (kJ mol^{-1})		E = 100 (kJ mol^{-1})		E = 125 (kJ mol^{-1})	
		κ_{est}	$\Delta\kappa$ (%)	κ_{est}	$\Delta\kappa$ (%)	κ_{est}	$\Delta\kappa$ (%)	κ_{est}	$\Delta\kappa$ (%)	κ_{est}	$\Delta\kappa$ (%)
4	406	4.000737	0.0184	4.235654	5.8913	4.577915	14.4479	5.574167	39.3542	6.243081	56.0770
	498	3.989294	-0.2677	4.069681	1.7420	4.292981	7.3245	5.077181	26.9295	5.625006	40.6252
	601	3.983388	-0.4153	3.961084	-0.9729	4.063568	1.5892	4.516548	12.9137	4.837134	20.9283
	705	3.978974	-0.5257	3.842285	-3.9429	3.802965	-4.9259	3.906156	-2.3461	4.016134	0.4033
	810	3.979979	-0.5005	3.833911	-4.1522	3.760848	-5.9788	3.760715	-5.9821	3.807754	-4.8061
6.5	406	6.505982	0.0920	6.825681	5.0105	7.310897	12.4753	8.756300	34.7123	9.735189	49.7721
	498	6.490587	-0.1448	6.542541	0.6545	6.830568	5.0857	7.947884	22.2751	8.747040	34.5699
	601	6.482825	-0.2642	6.373591	-1.9448	6.478781	-0.3264	7.105641	9.3176	7.570531	16.4697
	705	6.476277	-0.3650	6.192610	-4.7291	6.081829	-6.4334	6.178872	-4.9404	6.326499	-2.6692
	810	6.477781	-0.3418	6.188287	-4.7956	6.029278	-7.2419	5.970439	-8.1471	6.022763	-7.3421
10	406	10.015061	0.1506	10.416375	4.1638	11.062321	10.6232	13.052246	30.5225	14.419659	44.1966
	498	9.995834	-0.0417	9.959757	-0.4024	10.295107	2.9511	11.800629	18.0063	12.912732	29.1273
	601	9.986463	-0.1354	9.709457	-2.9054	9.781350	-2.1865	10.592437	5.9244	11.232697	12.3270
	705	9.977293	-0.2271	9.448492	-5.5151	9.207827	-7.9217	9.254030	-7.4597	9.437253	-5.6275
	810	9.979495	-0.2051	9.455922	-5.4408	9.150718	-8.4928	8.973295	-10.2671	9.018971	-9.8103

Appendix Table C1 (Continued)

$\kappa_{\xi=0.5}$	$T_{\xi=0.5}$ (K)	E = 1 (kJ mol^{-1})		E = 25 (kJ mol^{-1})		E = 50 (kJ mol^{-1})		E = 100 (kJ mol^{-1})		E = 125 (kJ mol^{-1})	
		κ_{est}	$\Delta\kappa$ (%)	κ_{est}	$\Delta\kappa$ (%)	κ_{est}	$\Delta\kappa$ (%)	κ_{est}	$\Delta\kappa$ (%)	κ_{est}	$\Delta\kappa$ (%)
15	406	15.030004	0.2000	15.504909	3.3661	16.335419	8.9028	19.010795	26.7386	20.885214	39.2348
	498	15.007260	0.0484	14.788455	-1.4103	15.140944	0.9396	17.114456	14.0964	18.633442	24.2229
	601	14.996830	-0.0211	14.424819	-3.8345	14.404362	-3.9709	15.410881	2.7392	16.272685	8.4846
	705	14.984363	-0.1042	14.057708	-6.2819	13.595090	-9.3661	13.518317	-9.8779	13.732966	-8.4469
	810	14.987551	-0.0830	14.089395	-6.0707	13.543750	-9.7083	13.153029	-12.3131	13.172805	-12.1813
28	406	28.073852	0.2638	28.622451	2.2230	29.810915	6.4676	34.024485	21.5160	37.095700	32.4846
	498	28.047259	0.1688	27.194000	-2.8786	27.451300	-1.9596	30.412183	8.6149	32.889957	17.4641
	601	28.037572	0.1342	26.540243	-5.2134	26.151759	-6.6009	27.478712	-1.8617	28.842172	3.0078
	705	28.017802	0.0636	25.919837	-7.4292	24.774451	-11.5198	24.235367	-13.4451	24.479819	-12.5721
	810	28.023551	0.0841	26.036388	-7.0129	24.773915	-11.5217	23.702521	-15.3481	23.609875	-15.6790

Appendix D

Simulated results for κ_{est} and $\Delta\kappa$ (%) obtained from the unit-area-normalized-response-fitting method at various $\kappa_{\xi=0.5}$ and E for different $T_{\xi=0.5}$.

Appendix Table D1 Simulated results for κ_{est} and $\Delta\kappa$ (%) obtained from the exit-flow-rate-curve-fitting method at various $\kappa_{\xi=0.5}$ and E for different $T_{\xi=0.5}$.

$\kappa_{\xi=0.5}$	$T_{\xi=0.5}$ (K)	E = 1 (kJ mol^{-1})		E = 25 (kJ mol^{-1})		E = 50 (kJ mol^{-1})		E = 100 (kJ mol^{-1})		E = 125 (kJ mol^{-1})	
		κ_{est}	$\Delta\kappa$(%)	κ_{est}	$\Delta\kappa$(%)	κ_{est}	$\Delta\kappa$(%)	κ_{est}	$\Delta\kappa$(%)	κ_{est}	$\Delta\kappa$(%)
0.02	406	0.023121	15.6028	0.025353	26.7662	0.028271	41.3549	0.036336	81.6816	0.041766	108.8322
	498	0.026659	33.2926	0.028389	41.9462	0.030767	53.8350	0.037453	87.2653	0.041931	109.6571
	601	0.027746	38.7292	0.028855	44.2733	0.030383	51.9141	0.034497	72.4854	0.037098	85.4881
	705	0.027680	38.4022	0.028024	40.1194	0.028602	43.0087	0.030287	51.4375	0.031363	56.8151
	810	0.027360	36.8005	0.027502	37.5109	0.027804	39.0204	0.028772	43.8618	0.029409	47.0463
0.04	406	0.043124	7.8110	0.047587	18.9678	0.053418	33.5440	0.069529	73.8223	0.080371	100.9279
	498	0.046586	16.4655	0.050044	25.1104	0.054795	36.9868	0.068150	70.3751	0.077093	92.7329
	601	0.047632	19.0792	0.049846	24.6161	0.052899	32.2478	0.061118	52.7947	0.066312	65.7803
	705	0.047536	18.8412	0.048221	20.5526	0.049375	23.4365	0.052741	31.8535	0.054890	37.2243
	810	0.047216	18.0400	0.047498	18.7456	0.048100	20.2509	0.050033	25.0833	0.051305	28.2637

Appendix Table D1 (Continued)

$\kappa_{\zeta=0.5}$	$T_{\zeta=0.5}$ (K)	E = 1 (kJ mol^{-1})		E = 25 (kJ mol^{-1})		E = 50 (kJ mol^{-1})		E = 100 (kJ mol^{-1})		E = 125 (kJ mol^{-1})	
		κ_{est}	$\Delta\kappa$(%)	κ_{est}	$\Delta\kappa$(%)	κ_{est}	$\Delta\kappa$(%)	κ_{est}	$\Delta\kappa$(%)	κ_{est}	$\Delta\kappa$(%)
0.06	406	0.063128	5.2128	0.069818	16.3627	0.078556	30.9267	0.102694	71.1563	0.118930	98.2173
	498	0.066513	10.8551	0.071695	19.4915	0.078813	31.3554	0.098821	64.7019	0.112215	87.0243
	601	0.067517	12.5276	0.070834	18.0571	0.075408	25.6798	0.087721	46.2022	0.095502	59.1707
	705	0.067392	12.3193	0.068415	14.0253	0.070142	16.9034	0.075185	25.3085	0.078404	30.6725
	810	0.067071	11.7849	0.067492	12.4861	0.068392	13.9868	0.071286	18.8105	0.073192	21.9864
0.1	406	0.103133	3.1329	0.114269	14.2686	0.128808	28.8083	0.168940	68.9401	0.195912	95.9116
	498	0.106364	6.3644	0.114983	14.9834	0.126822	26.8220	0.160084	60.0842	0.182337	82.3371
	601	0.107284	7.2836	0.112798	12.7984	0.120403	20.4028	0.140876	40.8761	0.153811	53.8108
	705	0.107099	7.0991	0.108794	8.7940	0.111661	11.6607	0.120042	20.0418	0.125392	25.3923
	810	0.106778	6.7784	0.107470	7.4704	0.108962	8.9621	0.113768	13.7684	0.116935	16.9351
0.25	406	0.253135	1.2540	0.280840	12.3361	0.316957	26.7829	0.416361	66.5444	0.482941	93.1764
	498	0.255778	2.3111	0.277161	10.8644	0.306519	22.6078	0.388875	55.5500	0.443845	77.5378
	601	0.256377	2.5509	0.270024	8.0097	0.288862	15.5448	0.339578	35.8314	0.371590	48.6362
	705	0.255969	2.3878	0.260101	4.0404	0.267160	6.8639	0.287885	15.1542	0.301134	20.4535
	810	0.255650	2.2602	0.257294	2.9176	0.260938	4.3751	0.272787	9.1150	0.280618	12.2473

Appendix Table D1 (Continued)

$\kappa_{\zeta=0.5}$	$T_{\zeta=0.5}$ (K)	E = 1 (kJ mol^{-1})		E = 25 (kJ mol^{-1})		E = 50 (kJ mol^{-1})		E = 100 (kJ mol^{-1})		E = 125 (kJ mol^{-1})	
		κ_{est}	$\Delta\kappa$(%)	κ_{est}	$\Delta\kappa$(%)	κ_{est}	$\Delta\kappa$(%)	κ_{est}	$\Delta\kappa$(%)	κ_{est}	$\Delta\kappa$(%)
0.45	406	0.453096	0.6880	0.502637	11.6972	0.567081	26.0179	0.743751	65.2780	0.861533	91.4517
	498	0.454927	1.0949	0.493014	9.5586	0.545275	21.1722	0.691562	53.6805	0.788891	75.3090
	601	0.455091	1.1313	0.479312	6.5137	0.512797	13.9548	0.602946	33.9881	0.659777	46.6172
	705	0.454386	0.9747	0.461563	2.5696	0.474002	5.3339	0.510753	13.5007	0.534287	18.7305
	810	0.454074	0.9053	0.456819	1.5153	0.463167	2.9261	0.484090	7.5755	0.497975	10.6611
0.7	406	0.702983	0.4262	0.779393	11.3418	0.878517	25.5024	1.148900	64.1285	1.328085	89.7264
	498	0.703758	0.5369	0.762202	8.8860	0.842337	20.3339	1.066045	52.2921	1.214266	73.4666
	601	0.703364	0.4805	0.740356	5.7651	0.791603	13.0861	0.929584	32.7977	1.016430	45.2043
	705	0.702289	0.3269	0.712933	1.8476	0.731753	4.5362	0.787818	12.5455	0.823803	17.6861
	810	0.701992	0.2846	0.705835	0.8336	0.715291	2.1845	0.747028	6.7182	0.768209	9.7441
1	406	1.002760	0.2760	1.110772	11.0772	1.250424	25.0424	1.629046	62.9046	1.878165	87.8165
	498	1.002211	0.2211	1.084294	8.4294	1.196754	19.6754	1.509676	50.9676	1.715975	71.5975
	601	1.001130	0.1130	1.052770	5.2770	1.124513	12.4513	1.317723	31.7723	1.439102	43.9102
	705	0.999609	-0.0391	1.013898	1.3898	1.039855	3.9855	1.118021	11.8021	1.168351	16.8351
	810	0.999342	-0.0658	1.004078	0.4078	1.016848	1.6848	1.060769	6.0769	1.090298	9.0298

Appendix Table D1 (Continued)

$\kappa_{\zeta=0.5}$	$T_{\zeta=0.5}$ (K)	E = 1 (kJ mol^{-1})		E = 25 (kJ mol^{-1})		E = 50 (kJ mol^{-1})		E = 100 (kJ mol^{-1})		E = 125 (kJ mol^{-1})	
		κ_{est}	$\Delta\kappa$(%)	κ_{est}	$\Delta\kappa$(%)	κ_{est}	$\Delta\kappa$(%)	κ_{est}	$\Delta\kappa$(%)	κ_{est}	$\Delta\kappa$(%)
1.5	406	1.502190	0.1460	1.661277	10.7518	1.865831	24.3888	2.414840	60.9893	2.771860	84.7907
	498	1.499310	-0.0460	1.618831	7.9221	1.782413	18.8275	2.235191	49.0127	2.531281	68.7521
	601	1.497035	-0.1976	1.571411	4.7608	1.675298	11.6865	1.955309	30.3540	2.130706	42.0470
	705	1.494783	-0.3478	1.513851	0.9234	1.550406	3.3604	1.662760	10.8507	1.735527	15.7018
	810	1.494589	-0.3607	1.499746	-0.0170	1.517006	1.1338	1.579268	5.2845	1.621709	8.1139
2	406	2.001401	0.0701	2.209550	10.4775	2.475733	23.7867	3.183201	59.1601	3.638215	81.9107
	498	1.996047	-0.1976	2.150525	7.5262	2.361808	18.0904	2.943809	47.1905	3.321545	66.0772
	601	1.992535	-0.3733	2.087506	4.3753	2.221012	11.0506	2.581410	29.0705	2.806597	40.3298
	705	1.989553	-0.5224	2.011745	0.5873	2.057256	2.8628	2.200487	10.0244	2.293874	14.6937
	810	1.989461	-0.5269	1.993670	-0.3165	2.014104	0.7052	2.092230	4.6115	2.146335	7.3168
2.8	406	2.799730	-0.0096	3.082247	10.0803	3.440499	22.8750	4.378887	56.3888	4.972881	77.6029
	498	2.790180	-0.3507	2.995459	6.9807	3.276181	17.0065	4.044506	44.4466	4.537949	62.0696
	601	2.784603	-0.5499	2.908083	3.8601	3.083839	10.1371	3.560241	27.1514	3.857053	37.7519
	705	2.780467	-0.6976	2.804183	0.1494	2.860620	2.1650	3.046536	8.8048	3.169295	13.1891
	810	2.780594	-0.6931	2.780411	-0.6996	2.803175	0.1134	2.901599	3.6285	2.971838	6.1371

Appendix Table D1 (Continued)

$\kappa_{\xi=0.5}$	$T_{\xi=0.5}$ (K)	E = 1 (kJ mol^{-1})		E = 25 (kJ mol^{-1})		E = 50 (kJ mol^{-1})		E = 100 (kJ mol^{-1})		E = 125 (kJ mol^{-1})	
		κ_{est}	$\Delta\kappa$(%)	κ_{est}	$\Delta\kappa$(%)	κ_{est}	$\Delta\kappa$(%)	κ_{est}	$\Delta\kappa$(%)	κ_{est}	$\Delta\kappa$(%)
4	406	3.996472	-0.0882	4.381406	9.5352	4.863902	21.5976	6.103831	52.5958	6.873231	71.8308
	498	3.980164	-0.4959	4.250269	6.2567	4.620449	15.5112	5.627033	40.6758	6.265734	56.6433
	601	3.971335	-0.7166	4.127642	3.1910	4.355611	8.8903	4.979766	24.4941	5.368032	34.2008
	705	3.965500	-0.8625	3.983656	-0.4086	4.048898	1.2224	4.284265	7.1066	4.443502	11.0876
	810	3.966067	-0.8483	3.952784	-1.1804	3.972887	-0.6778	4.090543	2.2636	4.179533	4.4883
6.5	406	6.487608	-0.1906	7.054871	8.5365	7.751963	19.2610	9.489854	45.9978	10.536684	62.1028
	498	6.456013	-0.6767	6.822159	4.9563	7.330619	12.7788	8.711217	34.0187	9.575225	47.3112
	601	6.439996	-0.9231	6.630187	2.0029	6.929638	6.6098	7.779917	19.6910	8.312015	27.8772
	705	6.430736	-1.0656	6.409656	-1.3899	6.467007	-0.5076	6.756974	3.9535	6.968087	7.2013
	810	6.432572	-1.0374	6.368975	-2.0158	6.362019	-2.1228	6.481594	-0.2832	6.591715	1.4110
10	406	9.972347	-0.2765	10.739595	7.3959	11.663669	16.6367	13.903460	39.0346	15.217928	52.1793
	498	9.917773	-0.8223	10.347820	3.4782	10.968204	9.6820	12.683378	26.8338	13.754024	37.5402
	601	9.891143	-1.0886	10.065284	0.6528	10.399014	3.9901	11.432346	14.3235	12.095787	20.9579
	705	9.877332	-1.2267	9.749501	-2.5050	9.747543	-2.5246	10.028920	0.2892	10.272648	2.7265
	810	9.881512	-1.1849	9.704214	-2.9579	9.619104	-3.8090	9.672683	-3.2732	9.781440	-2.1856

Appendix Table D1 (Continued)

$\kappa_{\xi=0.5}$	$T_{\xi=0.5}$ (K)	E = 1 (kJ mol^{-1})		E = 25 (kJ mol^{-1})		E = 50 (kJ mol^{-1})		E = 100 (kJ mol^{-1})		E = 125 (kJ mol^{-1})	
		κ_{est}	$\Delta\kappa$(%)	κ_{est}	$\Delta\kappa$(%)	κ_{est}	$\Delta\kappa$(%)	κ_{est}	$\Delta\kappa$(%)	κ_{est}	$\Delta\kappa$(%)
15	406	14.947550	-0.3497	15.923434	6.1562	17.075454	13.8364	19.797383	31.9826	21.358899	42.3927
	498	14.858623	-0.9425	15.279285	1.8619	15.948557	6.3237	17.906724	19.3782	19.147981	27.6532
	601	14.816285	-1.2248	14.874995	-0.8334	15.164676	1.0978	16.284553	8.5637	17.049853	13.6657
	705	14.796364	-1.3576	14.438822	-3.7412	14.280842	-4.7944	14.430394	-3.7974	14.667494	-2.2167
	810	14.804611	-1.3026	14.400588	-3.9961	14.144357	-5.7043	14.003900	-6.6407	14.067640	-6.2157
28	406	27.876080	-0.4426	29.156420	4.1301	30.616138	9.3433	33.933875	21.1924	35.775736	27.7705
	498	27.694620	-1.0906	27.769621	-0.8228	28.219873	0.7853	30.122211	7.5793	31.466228	12.3794
	601	27.610238	-1.3920	27.064065	-3.3426	26.936168	-3.7994	27.739136	-0.9317	28.520699	1.8596
	705	27.575901	-1.5146	26.363489	-5.8447	25.558033	-8.7213	24.970279	-10.8204	25.025075	-10.6247
	810	27.596697	-1.4404	26.389405	-5.7521	25.484859	-8.9826	24.504894	-12.4825	24.312962	-13.1680

Appendix E

Simulated results for κ_{est} and $\Delta\kappa$ (%) obtained from the conversion-expression-using method at various $\kappa_{\xi=0.5}$ and E for different $T_{\xi=0.5}$.

Appendix Table E1 Simulated results for κ_{est} and $\Delta\kappa$ (%) obtained from the conversion-expression-using method at various $\kappa_{\xi=0.5}$ and E for different $T_{\xi=0.5}$.

$\kappa_{\xi=0.5}$	$T_{\xi=0.5}$ (K)	E = 1 (kJ mol^{-1})		E = 25 (kJ mol^{-1})		E = 50 (kJ mol^{-1})		E = 100 (kJ mol^{-1})		E = 125 (kJ mol^{-1})	
		κ_{est}	$\Delta\kappa$ (%)	κ_{est}	$\Delta\kappa$ (%)	κ_{est}	$\Delta\kappa$ (%)	κ_{est}	$\Delta\kappa$ (%)	κ_{est}	$\Delta\kappa$ (%)
0.02	406	0.019157	-4.2135	0.020953	4.7674	0.023430	17.1478	0.030558	52.7879	0.035447	77.2369
	498	0.019919	-0.4032	0.021096	5.4805	0.023005	15.0232	0.028833	44.1675	0.032849	64.2429
	601	0.019935	-0.3225	0.020528	2.6386	0.021663	8.3129	0.025162	25.8117	0.027474	37.3714
	705	0.019818	-0.9118	0.019716	-1.4184	0.019973	-0.1336	0.021216	6.0808	0.022112	10.5598
	810	0.019870	-0.6507	0.019632	-1.8418	0.019651	-1.7457	0.020233	1.1663	0.020722	3.6109
0.04	406	0.039215	-1.9626	0.042800	7.0004	0.047742	19.3551	0.061964	54.9097	0.071714	79.2860
	498	0.039953	-0.1171	0.042298	5.7441	0.046105	15.2613	0.057733	44.3318	0.065740	64.3503
	601	0.039948	-0.1308	0.041124	2.8101	0.043386	8.4651	0.050368	25.9201	0.054980	37.4511
	705	0.039804	-0.4908	0.039594	-1.0140	0.040103	0.2574	0.042579	6.4486	0.044366	10.9156
	810	0.039853	-0.3669	0.039371	-1.5718	0.039405	-1.4869	0.040563	1.4071	0.041537	3.8436

Appendix Table E1 (Continued)

$\kappa_{\zeta=0.5}$	$T_{\zeta=0.5}$ (K)	E = 1 (kJ mol^{-1})		E = 25 (kJ mol^{-1})		E = 50 (kJ mol^{-1})		E = 100 (kJ mol^{-1})		E = 125 (kJ mol^{-1})	
		κ_{est}	$\Delta\kappa$ (%)	κ_{est}	$\Delta\kappa$ (%)	κ_{est}	$\Delta\kappa$ (%)	κ_{est}	$\Delta\kappa$ (%)	κ_{est}	$\Delta\kappa$ (%)
0.06	406	0.059273	-1.2120	0.064640	7.7329	0.072037	20.0624	0.093319	55.5320	0.107902	79.8363
	498	0.059987	-0.0212	0.063491	5.8178	0.069186	15.3094	0.086584	44.3069	0.098561	64.2689
	601	0.059960	-0.0661	0.061713	2.8548	0.065094	8.4905	0.075541	25.9018	0.082443	37.4047
	705	0.059790	-0.3496	0.059467	-0.8890	0.060221	0.3690	0.063922	6.5370	0.066595	10.9921
	810	0.059837	-0.2714	0.059106	-1.4900	0.059150	-1.4162	0.060876	1.4599	0.062333	3.8883
0.1	406	0.099389	-0.6110	0.108298	8.2981	0.120578	20.5775	0.155879	55.8789	0.180042	80.0416
	498	0.100057	0.0569	0.105851	5.8513	0.115292	15.2921	0.144145	44.1455	0.163996	63.9960
	601	0.099987	-0.0129	0.102868	2.8684	0.108466	8.4657	0.125790	25.7905	0.137238	37.2378
	705	0.099765	-0.2349	0.099193	-0.8067	0.100425	0.4247	0.106547	6.5467	0.110978	10.9782
	810	0.099807	-0.1932	0.098561	-1.4391	0.098613	-1.3874	0.101453	1.4533	0.103865	3.8652
0.25	406	0.249831	-0.0676	0.271774	8.7094	0.302016	20.8062	0.388747	55.4987	0.447885	79.1541
	498	0.250331	0.1323	0.264409	5.7636	0.287547	15.0187	0.358372	43.3488	0.406997	62.7989
	601	0.250105	0.0421	0.256942	2.7770	0.270584	8.2336	0.313108	25.2432	0.341223	36.4893
	705	0.249690	-0.1240	0.247962	-0.8152	0.250797	0.3187	0.265681	6.2722	0.276544	10.6175
	810	0.249713	-0.1149	0.246347	-1.4613	0.246273	-1.4908	0.253050	1.2200	0.258930	3.5720

Appendix Table E1 (Continued)

$\kappa_{\zeta=0.5}$	$T_{\zeta=0.5}$ (K)	E = 1 (kJ mol^{-1})		E = 25 (kJ mol^{-1})		E = 50 (kJ mol^{-1})		E = 100 (kJ mol^{-1})		E = 125 (kJ mol^{-1})	
		κ_{est}	$\Delta\kappa$ (%)	κ_{est}	$\Delta\kappa$ (%)	κ_{est}	$\Delta\kappa$ (%)	κ_{est}	$\Delta\kappa$ (%)	κ_{est}	$\Delta\kappa$ (%)
0.45	406	0.450435	0.0967	0.489168	8.7040	0.542556	20.5680	0.695244	54.4986	0.798890	77.5310
	498	0.450727	0.1616	0.475123	5.5830	0.515705	14.6011	0.640234	42.2742	0.725535	61.2300
	601	0.450305	0.0677	0.461763	2.6139	0.485507	7.8905	0.560254	24.5009	0.609728	35.4952
	705	0.449636	-0.0808	0.445832	-0.9262	0.450370	0.0823	0.476192	5.8204	0.495254	10.0564
	810	0.449635	-0.0812	0.442992	-1.5574	0.442388	-1.6915	0.453837	0.8526	0.464077	3.1282
0.7	406	0.701212	0.1732	0.760046	8.5780	0.841170	20.1672	1.072518	53.2168	1.228813	75.5446
	498	0.701270	0.1815	0.737464	5.3520	0.798628	14.0897	0.987001	41.0002	1.115753	59.3933
	601	0.700617	0.0881	0.716860	2.4086	0.752297	7.4711	0.865296	23.6137	0.940217	34.3168
	705	0.699639	-0.0515	0.692428	-1.0818	0.698437	-0.2232	0.736817	5.2595	0.765568	9.3669
	810	0.699609	-0.0558	0.688186	-1.6877	0.686371	-1.9470	0.702790	0.3986	0.718086	2.5837
1	406	1.002176	0.2176	1.083922	8.3922	1.196730	19.6730	1.517570	51.7570	1.733310	73.3310
	498	1.001988	0.1988	1.050836	5.0836	1.135060	13.5060	1.395768	39.5768	1.573639	57.3639
	601	1.001079	0.1079	1.021708	2.1708	1.069912	6.9912	1.226131	22.6131	1.329970	32.9970
	705	0.999740	-0.0260	0.987325	-1.2675	0.994205	-0.5795	1.046152	4.6152	1.085788	8.5788
	810	0.999678	-0.0322	0.981579	-1.8421	0.977559	-2.2441	0.998764	-0.1236	1.019598	1.9598

Appendix Table E1 (Continued)

$\kappa_{\zeta=0.5}$	$T_{\zeta=0.5}$ (K)	E = 1 (kJ mol^{-1})		E = 25 (kJ mol^{-1})		E = 50 (kJ mol^{-1})		E = 100 (kJ mol^{-1})		E = 125 (kJ mol^{-1})	
		κ_{est}	$\Delta\kappa$ (%)	κ_{est}	$\Delta\kappa$ (%)	κ_{est}	$\Delta\kappa$ (%)	κ_{est}	$\Delta\kappa$ (%)	κ_{est}	$\Delta\kappa$ (%)
1.5	406	1.503849	0.2566	1.621135	8.0756	1.783316	18.8877	2.243218	49.5479	2.550657	70.0438
	498	1.503328	0.2219	1.569970	4.6647	1.689090	12.6060	2.061475	37.4317	2.315172	54.3448
	601	1.502041	0.1360	1.526991	1.7994	1.593721	6.2481	1.816296	21.0864	1.965002	31.0001
	705	1.500120	0.0080	1.476570	-1.5620	1.482928	-1.1381	1.554234	3.6156	1.610431	7.3621
	810	1.500010	0.0007	1.468709	-2.0861	1.459355	-2.7097	1.485962	-0.9359	1.514882	0.9921
2	406	2.005599	0.2799	2.155485	7.7742	2.363321	18.1660	2.951821	47.5911	3.343647	67.1823
	498	2.004831	0.2415	2.085591	4.2796	2.235755	11.7878	2.710529	35.5265	3.033993	51.6996
	601	2.003219	0.1609	2.029145	1.4572	2.111372	5.5686	2.394240	19.7120	2.584362	29.2181
	705	2.000741	0.0370	1.963288	-1.8356	1.966927	-1.6536	2.054026	2.7013	2.125085	6.2543
	810	2.000589	0.0295	1.953749	-2.3126	1.937206	-3.1397	1.966366	-1.6817	2.002125	0.1063
2.8	406	2.808535	0.3048	3.005348	7.3338	3.279795	17.1355	4.056840	44.8871	4.572257	63.2949
	498	2.807528	0.2689	2.904304	3.7251	3.097419	10.6221	3.720578	32.8778	4.146075	48.0741
	601	2.805495	0.1963	2.826964	0.9630	2.928635	4.5941	3.297638	17.7728	3.548358	26.7271
	705	2.802168	0.0774	2.737470	-2.2332	2.732818	-2.3993	2.838915	1.3898	2.930835	4.6727
	810	2.801960	0.0700	2.726035	-2.6416	2.694649	-3.7625	2.722824	-2.7563	2.767346	-1.1662

Appendix Table E1 (Continued)

$\kappa_{\zeta=0.5}$	$T_{\zeta=0.5}$ (K)	E = 1 (kJ mol^{-1})		E = 25 (kJ mol^{-1})		E = 50 (kJ mol^{-1})		E = 100 (kJ mol^{-1})		E = 125 (kJ mol^{-1})	
		κ_{est}	$\Delta\kappa$ (%)	κ_{est}	$\Delta\kappa$ (%)	κ_{est}	$\Delta\kappa$ (%)	κ_{est}	$\Delta\kappa$ (%)	κ_{est}	$\Delta\kappa$ (%)
4	406	4.013202	0.3300	4.270490	6.7623	4.633044	15.8261	5.663040	41.5760	6.345081	58.6270
	498	4.012139	0.3035	4.120407	3.0102	4.365499	9.1375	5.184128	29.6032	5.746705	43.6676
	601	4.009664	0.2416	4.012903	0.3226	4.133668	3.3417	4.613203	15.3301	4.945001	23.6250
	705	4.005147	0.1287	3.889936	-2.7516	3.865303	-3.3674	3.988160	-0.2960	4.106056	2.6514
	810	4.004873	0.1218	3.877174	-3.0706	3.817094	-4.5727	3.834175	-4.1456	3.887787	-2.8053
6.5	406	6.523681	0.3643	6.878966	5.8302	7.393088	13.7398	8.874714	36.5341	9.859697	51.6876
	498	6.523367	0.3595	6.619852	1.8439	6.938976	6.7535	8.095278	24.5427	8.905219	37.0034
	601	6.520529	0.3158	6.452530	-0.7303	6.584745	1.3038	7.244776	11.4581	7.720757	18.7809
	705	6.513776	0.2119	6.265338	-3.6102	6.177345	-4.9639	6.302288	-3.0417	6.459999	-0.6154
	810	6.513420	0.2065	6.254199	-3.7816	6.115709	-5.9122	6.082297	-6.4262	6.143623	-5.4827
10	406	10.039500	0.3950	10.490238	4.9024	11.170901	11.7090	13.184830	31.8483	14.539225	45.3922
	498	10.041562	0.4156	10.067525	0.6752	10.440315	4.4031	11.975125	19.7513	13.083341	30.8334
	601	10.039086	0.3909	9.820339	-1.7966	9.926090	-0.7391	10.768344	7.6834	11.413343	14.1334
	705	10.029581	0.2958	9.551314	-4.4869	9.341129	-6.5887	9.419983	-5.8002	9.613029	-3.8697
	810	10.029189	0.2919	9.549245	-4.5076	9.272107	-7.2789	9.126314	-8.7369	9.181888	-8.1811

Appendix Table E1 (Continued)

$\kappa_{\zeta=0.5}$	$T_{\zeta=0.5}$ (K)	E = 1 (kJ mol^{-1})		E = 25 (kJ mol^{-1})		E = 50 (kJ mol^{-1})		E = 100 (kJ mol^{-1})		E = 125 (kJ mol^{-1})	
		κ_{est}	$\Delta\kappa$ (%)	κ_{est}	$\Delta\kappa$ (%)	κ_{est}	$\Delta\kappa$ (%)	κ_{est}	$\Delta\kappa$ (%)	κ_{est}	$\Delta\kappa$ (%)
15	406	15.063501	0.4233	15.600357	4.0024	16.466096	9.7740	19.131799	27.5453	20.957783	39.7186
	498	15.070596	0.4706	14.929557	-0.4696	15.319482	2.1299	17.290043	15.2670	18.774459	25.1631
	601	15.069753	0.4650	14.571914	-2.8539	14.587583	-2.7494	15.607944	4.0530	16.458436	9.7229
	705	15.056798	0.3787	14.195596	-5.3627	13.768556	-8.2096	13.721426	-8.5238	13.941083	-7.0594
	810	15.056443	0.3763	14.215105	-5.2326	13.703281	-8.6448	13.344811	-11.0346	13.372155	-10.8523
28	406	28.129784	0.4635	28.753060	2.6895	29.959725	6.9990	34.043818	21.5851	36.957917	31.9926
	498	28.154573	0.5520	27.393199	-2.1671	27.663280	-1.2026	30.491137	8.8969	32.829565	17.2484
	601	28.161308	0.5761	26.753983	-4.4501	26.385198	-5.7672	27.641820	-1.2792	28.953529	3.4055
	705	28.140779	0.5028	26.125001	-6.6964	25.009677	-10.6797	24.461949	-12.6359	24.685421	-11.8378
	810	28.140752	0.5027	26.226015	-6.3357	24.996072	-10.7283	23.932203	-14.5278	23.829547	-14.8945

Appendix F

Simulated results for κ_{est} and $\Delta\kappa$ (%) obtained from the mean-residence-time-expression-using method at various $\kappa_{\xi=0.5}$ and E for different $T_{\xi=0.5}$.

Appendix Table F1 Simulated results for κ_{est} and $\Delta\kappa$ (%) obtained from the mean-residence-time-using method at various $\kappa_{\xi=0.5}$ and E for different $T_{\xi=0.5}$.

$\kappa_{\xi=0.5}$	$T_{\xi=0.5}$ (K)	E = 1 (kJ mol^{-1})		E = 25 (kJ mol^{-1})		E = 50 (kJ mol^{-1})		E = 100 (kJ mol^{-1})		E = 125 (kJ mol^{-1})	
		κ_{est}	$\Delta\kappa$ (%)	κ_{est}	$\Delta\kappa$ (%)	κ_{est}	$\Delta\kappa$ (%)	κ_{est}	$\Delta\kappa$ (%)	κ_{est}	$\Delta\kappa$ (%)
0.06	406	0.079297	32.1621	0.086141	43.5682	0.095057	58.4281	0.119633	99.3875	0.136147	126.9113
	498	0.074899	24.8319	0.080238	33.7302	0.087519	45.8652	0.107896	79.8275	0.121515	102.5252
	601	0.068759	14.5985	0.072198	20.3306	0.076885	28.1409	0.089413	49.0215	0.097309	62.1819
	705	0.057891	-3.5147	0.059003	-1.6612	0.060801	1.3349	0.065955	9.9249	0.069222	15.3698
	810	0.055340	-7.7668	0.055838	-6.9368	0.056797	-5.3383	0.059783	-0.3616	0.061728	2.8798
0.1	406	0.119681	19.6812	0.131077	31.0773	0.145918	45.9179	0.186798	86.7976	0.214245	114.2455
	498	0.115062	15.0616	0.123947	23.9471	0.136063	36.0634	0.169959	69.9586	0.192600	92.6002
	601	0.108730	8.7304	0.114454	14.4538	0.122249	22.2490	0.143092	43.0916	0.156224	56.2237
	705	0.097608	-2.3924	0.099453	-0.5468	0.102441	2.4414	0.111013	11.0130	0.116448	16.4477
	810	0.095007	-4.9925	0.095828	-4.1724	0.097424	-2.5762	0.102388	2.3878	0.105620	5.6199

Appendix Table F1 (Continued)

$\kappa_{\zeta=0.5}$	$T_{\zeta=0.5}$ (K)	E = 1 (kJ mol^{-1})		E = 25 (kJ mol^{-1})		E = 50 (kJ mol^{-1})		E = 100 (kJ mol^{-1})		E = 125 (kJ mol^{-1})	
		κ_{est}	$\Delta\kappa$ (%)	κ_{est}	$\Delta\kappa$ (%)	κ_{est}	$\Delta\kappa$ (%)	κ_{est}	$\Delta\kappa$ (%)	κ_{est}	$\Delta\kappa$ (%)
0.25	406	0.271113	8.4452	0.299512	19.8047	0.336437	34.5748	0.437874	75.1498	0.505777	102.3108
	498	0.265653	6.2610	0.287753	15.1011	0.317863	27.1452	0.401960	60.7840	0.458019	83.2074
	601	0.258598	3.4393	0.272810	9.1238	0.292167	16.8669	0.343902	37.5608	0.376469	50.5878
	705	0.246511	-1.3957	0.251056	0.4222	0.258449	3.3797	0.279706	11.8824	0.293193	17.2772
	810	0.243730	-2.5082	0.245724	-1.7105	0.249653	-0.1390	0.261942	4.7766	0.269957	7.9830
0.45	406	0.473009	5.1132	0.523901	16.4224	0.589929	31.0954	0.770654	71.2565	0.891115	98.0255
	498	0.466393	3.6429	0.505895	12.4212	0.559648	24.3662	0.709441	57.6536	0.809005	79.7790
	601	0.458357	1.8572	0.483701	7.4891	0.518226	15.1614	0.610437	35.6527	0.668408	48.5350
	705	0.444972	-1.1174	0.452979	0.6621	0.466096	3.5770	0.503934	11.9854	0.527963	17.3251
	810	0.441949	-1.7891	0.445398	-1.0226	0.452324	0.5165	0.474142	5.3648	0.488410	8.5356
0.7	406	0.725361	3.6230	0.804070	14.8672	0.905910	29.4157	1.183327	69.0467	1.367207	95.3153
	498	0.717249	2.4642	0.778133	11.1618	0.860857	22.9796	1.090722	55.8175	1.242924	77.5606
	601	0.707961	1.1373	0.746908	6.7012	0.799974	14.2820	0.941593	34.5133	1.030475	47.2106
	705	0.692931	-1.0099	0.705037	0.7196	0.725057	3.5796	0.783065	11.8665	0.819956	17.1365
	810	0.689606	-1.4848	0.694688	-0.7588	0.705167	0.7381	0.738501	5.5001	0.760374	8.6248

Appendix Table F1 (Continued)

$\kappa_{\zeta=0.5}$	$T_{\zeta=0.5}$ (K)	E = 1 (kJ mol^{-1})		E = 25 (kJ mol^{-1})		E = 50 (kJ mol^{-1})		E = 100 (kJ mol^{-1})		E = 125 (kJ mol^{-1})	
		κ_{est}	$\Delta\kappa$ (%)	κ_{est}	$\Delta\kappa$ (%)	κ_{est}	$\Delta\kappa$ (%)	κ_{est}	$\Delta\kappa$ (%)	κ_{est}	$\Delta\kappa$ (%)
1	406	1.028154	2.8154	1.139782	13.9782	1.283741	28.3741	1.673562	67.3562	1.930151	93.0151
	498	1.018176	1.8176	1.104157	10.4157	1.220760	22.0760	1.543611	54.3611	1.756352	75.6352
	601	1.007347	0.7347	1.062140	6.2140	1.136820	13.6820	1.335938	33.5938	1.460643	46.0643
	705	0.990314	-0.9686	1.006987	0.6987	1.034904	3.4904	1.116283	11.6283	1.168114	16.8114
	810	0.986631	-1.3369	0.993388	-0.6612	1.007827	0.7827	1.054380	5.4380	1.085058	8.5058
1.5	406	1.532739	2.1826	1.698076	13.2051	1.910076	27.3384	2.478308	65.2205	2.847876	89.8584
	498	1.519489	1.2993	1.645856	9.7237	1.816715	21.1143	2.286848	52.4565	2.594066	72.9377
	601	1.506009	0.4006	1.585994	5.7330	1.695100	13.0067	1.985592	32.3728	2.166860	44.4573
	705	1.485575	-0.9617	1.508949	0.5966	1.549059	3.2706	1.667263	11.1509	1.742777	16.1851
	810	1.481298	-1.2468	1.490107	-0.6595	1.510393	0.6929	1.577454	5.1636	1.622003	8.1336
2	406	2.037243	1.8621	2.254768	12.7384	2.532059	26.6029	3.267576	63.3788	3.740181	87.0091
	498	2.020528	1.0264	2.185416	9.2708	2.407683	20.3842	3.015406	50.7703	3.409190	70.4595
	601	2.004306	0.2153	2.107893	5.3947	2.249362	12.4681	2.625561	31.2780	2.859455	42.9728
	705	1.980397	-0.9801	2.009279	0.4639	2.060309	3.0155	2.212612	10.6306	2.310253	15.5126
	810	1.975532	-1.2234	1.985421	-0.7289	2.010561	0.5281	2.096155	4.8078	2.153540	7.6770

Appendix Table F1 (Continued)

$\kappa_{\xi=0.5}$	$T_{\xi=0.5}$ (K)	E = 1 (kJ mol^{-1})		E = 25 (kJ mol^{-1})		E = 50 (kJ mol^{-1})		E = 100 (kJ mol^{-1})		E = 125 (kJ mol^{-1})	
		κ_{est}	$\Delta\kappa$ (%)	κ_{est}	$\Delta\kappa$ (%)	κ_{est}	$\Delta\kappa$ (%)	κ_{est}	$\Delta\kappa$ (%)	κ_{est}	$\Delta\kappa$ (%)
2.8	406	2.844281	1.5815	3.142054	12.2162	3.518045	25.6445	4.498813	60.6719	5.117099	82.7535
	498	2.821677	0.7742	3.044167	8.7202	3.342680	19.3814	4.150768	48.2417	4.667460	66.6950
	601	2.800889	0.0318	2.938799	4.9571	3.127684	11.7030	3.629255	29.6162	3.939374	40.6919
	705	2.771288	-1.0254	2.806381	0.2279	2.872149	2.5767	3.073219	9.7578	3.202996	14.3927
	810	2.765505	-1.2320	2.774994	-0.8931	2.805749	0.2053	2.916759	4.1700	2.992491	6.8747
4	406	4.054477	1.3619	4.464995	11.6249	4.976049	24.4012	6.276981	56.9245	7.075389	76.8847
	498	4.022351	0.5588	4.321796	8.0449	4.721002	18.0250	5.786696	44.6674	6.455657	61.3914
	601	3.994371	-0.1407	4.175621	4.3905	4.425583	10.6396	5.089038	27.2260	5.496376	37.4094
	705	3.955986	-1.1003	3.994196	-0.1451	4.075634	1.8908	4.336522	8.4131	4.507143	12.6786
	810	3.948863	-1.2784	3.952678	-1.1830	3.986756	-0.3311	4.126017	3.1504	4.224226	5.6057
6.5	406	6.574497	1.1461	7.191616	10.6402	7.938511	22.1309	9.754797	50.0738	10.818202	66.4339
	498	6.520498	0.3154	6.944909	6.8448	7.505090	15.4629	8.966813	37.9510	9.857102	51.6477
	601	6.476559	-0.3606	6.717452	3.3454	7.057904	8.5831	7.968924	22.5988	8.523735	31.1344
	705	6.419225	-1.2427	6.440137	-0.9210	6.529960	0.4609	6.866857	5.6440	7.096846	9.1822
	810	6.409492	-1.3924	6.403531	-1.4841	6.403531	-1.4841	6.564837	0.9975	6.691610	2.9478

Appendix Table F1 (Continued)

$\kappa_{\zeta=0.5}$	$T_{\zeta=0.5}$ (K)	E = 1 (kJ mol^{-1})		E = 25 (kJ mol^{-1})		E = 50 (kJ mol^{-1})		E = 100 (kJ mol^{-1})		E = 125 (kJ mol^{-1})	
		κ_{est}	$\Delta\kappa$ (%)	κ_{est}	$\Delta\kappa$ (%)	κ_{est}	$\Delta\kappa$ (%)	κ_{est}	$\Delta\kappa$ (%)	κ_{est}	$\Delta\kappa$ (%)
10	406	10.100314	1.0031	10.950476	9.5048	11.944050	19.4405	14.237589	42.3759	15.516452	55.1645
	498	10.012631	0.1263	10.540842	5.4084	11.234355	12.3435	13.014870	30.1487	14.073246	40.7325
	601	9.944953	-0.5505	10.206645	2.0664	10.602204	6.0220	11.699307	16.9931	12.370698	23.7070
	705	9.860297	-1.3970	9.807414	-1.9259	9.860297	-1.3970	10.208281	2.0828	10.474044	4.7404
	810	9.847256	-1.5274	9.734774	-2.6523	9.698771	-3.0123	9.817241	-1.8276	9.948880	-0.5112
15	406	15.133997	0.8933	16.230033	8.2002	17.458011	16.3867	20.134837	34.2322	21.556690	43.7113
	498	15.000000	0.0000	15.558816	3.7254	16.307464	8.7164	18.240996	21.6066	19.382273	29.2152
	601	14.891695	-0.7220	15.081806	0.5454	15.445710	2.9714	16.585809	10.5721	17.312175	15.4145
	705	14.767407	-1.5506	14.527098	-3.1527	14.444745	-3.7017	14.665567	-2.2296	14.914997	-0.5667
	810	14.750289	-1.6647	14.448778	-3.6748	14.264242	-4.9051	14.204032	-5.3065	14.289459	-4.7369
28	406	28.211559	0.7556	29.658629	5.9237	31.141395	11.2193	34.032158	21.5434	35.442923	26.5819
	498	28.000000	0.0000	28.201802	0.7207	28.660893	2.3603	30.147809	7.6707	31.126022	11.1644
	601	27.732186	-0.9565	27.283480	-2.5590	27.283480	-2.5590	27.852242	-0.5277	28.420353	1.5013
	705	27.504966	-1.7680	26.479571	-5.4301	25.755387	-8.0165	25.147845	-10.1863	25.144732	-10.1974
	810	27.479507	-1.8589	26.439761	-5.5723	25.626138	-8.4781	24.683507	-11.8446	24.471770	-12.6008

CURRICULUM VITAE

NAME : Miss Kaew-arpha Thavornprasert

BIRTH DATE : June 21, 1984

BIRTH PLACE : Nonthaburi, Thailand

EDUCATION :

YEAR	INSTITUTE	DEGREE/DIPLOMA
2005	Kasetsart Univ.	B.Sc. (Chemistry)
2010	Kasetsart Univ.	M.Eng. (Chemical Engineering)

SCHOLARSHIP : The National Center of Excellence for Petroleum, Petrochemicals, and Advanced Materials, Department of Chemical Engineering, Faculty of Engineering, Kasetsart University Scholarship 2005-2007